University of Belgrade
Faculty of Physics

Master Thesis

Classical and quantum chaos in the scattering of highly excited strings

Author:
Nikola Savić

Supervisors:
Dr. Mihailo Čubrović
Prof. Dr. Marija Dimitrijević-Ćirić

June, 2023
Belgrade

Univerzitet u Beogradu
Fizički fakultet

Master rad

Klasični i kvantni haos u rasejanju visoko ekscitovanih struna

Autor:
Nikola Savić

Mentori:
Dr Mihailo Čubrović
Prof Dr Marija Dimitrijević-Ćirić

Jun, 2023.
Beograd

Abstract

The correspondence between black holes and strings provides a way to study black holes through the physics of highly excited strings at weak coupling. In this thesis, we investigate the scattering of highly excited strings from classical and quantum perspective. Classically, we consider the scattering of a closed string on a Schwarzschild black hole. At the quantum level, we consider string-string scattering amplitudes, both for open and closed strings. We focus on the signs of chaos in the amplitudes which, due to the string/black hole correspondence, allows us to probe the chaoticity of black holes beyond the semi-classical regime. The large number of states of the highly excited string yields also some analytic understanding of the statistical properties of the string dynamics. In the S-matrix we observe a crossover from the low-energy regime in which short partitions determine the dynamics, to the high-energy regime when long partition states dominate. We analyze the distribution of eigenphase spacings and find decent agreement with the predictions of random matrix theory predictions for closed strings, which further corroborates the chaotic nature of the scattering.

Sažetak

Korespondencija između crnih rupa i struna omogućava proučavanje crnih rupa kroz fiziku visoko ekscitovanih struna u režimu slabe interakcije. U ovoj tezi istražili smo procese rasejanja visoko ekscitovanih struna u klasičnom i kvantnom režimu. Klasično, razmotrili smo rasejanje zatvorene strune na Švarcšildovoj crnoj rupi. Na kvantnom nivou, razmatrali smo amplitude rasejanja struna za otvorene i za zatvorene strune. Fokusirali smo se na znake haotičnosti u amplitudama koje zbog korespodencije između crnih rupa i struna omogućavaju ispitivanje haotičnosti crnih rupa izvan semiklasičnog režima. Veliki broj stanja visoko ekscitovane strune takođe pruža uvid u statističke osobine dinamike struna. Na nivou S-matrice primetili smo prelaz iz niskoenergetskog režima u kome kratke particije određuju dinamiku u visokoenergetski režim u kome su dominantna stanja dugih particija. Analizirali smo raspodelu svojstvenih faza i ustanovili zadovoljavajuće slaganje sa predviđanjima teorije nasumičnih matrica u slučaju zatvorenih struna, što ukazuje na haotičnost rasejanja koje razmatramo.

Acknowledgements

First of all, I would like to thank my supervisor Dr Mihailo Čubrović for guidance and support through every segment of work on this master thesis, whose enthusiasm, dedication and patience made it not just valuable, but also an enjoyable and fulfilling experience. I am grateful for all the knowledge he shared with me, the lessons which will follow me in my future scientific career and for all the time he selflessly devoted to our discussions. In addition, I am grateful to Professor Dr Marija Dimitrijević-Ćirić for supervising the work, useful discussions and comments on the manuscript.

Finally, I would like to thank my family and friends for supporting me to pursue my goals. My warmest thanks go to Anđela, for her inexhaustible support and being the main source of my happiness.

Contents

Chapter 1

Introduction

The black holes (BHs) are among the most studied objects in modern physics. One of the reasons is that, despite their simplicity at the classical level, quantum gravity is required to describe them fully consistently. Even though a lot can be learned from the effective field theory approach, which provides us with the perturbative description of gravity, to describe the most interesting features of black holes, like the singularity and scrambling, quantum treatment is needed. Hence the rich phenomenology of black holes provides important clues about the very nature of gravity, and any candidate for the theory of quantum gravity shall reproduce it (e.g. deriving the area law for BH entropy from counting the microscopic degrees of freedom). Furthermore, thanks to the AdS/CFT correspondence (gauge/gravity duality), BH physics provides a new perspective on unconventional materials described by condensed matter models which admit a holographic dual. In addition, their interesting causal structure and the related Black hole information paradox have provided a fertile ground to apply and develop some fundamental concepts of quantum information theory.

Recent developments in relation to the BH information paradox have resulted in the recognition that the BHs exhibit signs of *chaotic* behavior [1]. This is easily understood by thinking of the black hole evolution as a scattering process. The incoming state represents a large number of particles which collide in a small enough region of space to form an intermediate state which classically corresponds to a black hole. The black hole emits Hawking radiation which represents the outgoing state. Now if we change the incoming state by adding another particle of mass m, the BH mass will shift linearly from M to $M+m$[1] together with its horizon radius $r_s = 2M$ which shifts to $r_s + \delta = r_s + 2m$. One can show that the time it takes a Hawking quantum to escape from the distance $r = r_s + \delta$ is equal to $\frac{1}{2\pi T}\log\left(\frac{r_s}{\delta}\right)$ in the Schwarzschild coordinates, where T is the BH temperature. Upon the slight increase of r_s by $2m$ the escape time changes by $\Delta t = 2me^{2\pi Tt}$.

Thus, a small change in the initial conditions causes an exponentially enlarged change in the dynamics of outgoing particles the defining manifestation of chaotic behavior. This was thoroughly investigated in the semiclassical regime, where *out of time ordered correlators* were used to calculate the black hole Lyapunov exponent λ - the inverse of the time needed for two initially close orbits to separate by a factor of e. A remarkably simple result is obtained [1, 2, 3, 4, 5]:

$$\lambda = 2\pi T. \tag{1.1}$$

[1]Here we assume that the $m \ll M$ ensuring that the change of the incoming state is small.

The absence of any black hole parameters except the temperature T in the above expression suggests its universality, and indeed in [4] this value is proven to be the upper bound to the Lyapunov exponent in a broad class of systems. Another clue comes from the *fast scrambling* hypothesis, that the black holes are the fastest scramblers of information. By definition, the scrambling time is the time it takes for a local perturbation (or equivalently for some amount of information) to spread all over the system. Fast scrambling thus means that the time needed to redistribute the information entering the BH throughout its interior is shorter than for any other system of the same volume [1, 6]. These two results indicate the existence of a chaos-driving mechanism similar to the usual one in classical mechanics, that is *stretching and folding* of the phase space. Nevertheless, the Lyapunov exponent is only a crude characterization of chaotic behavior. It would be interesting to study the BH chaos further, and in particular to explore it beyond the semi-classical regime.

Another important and related issue is understanding the chaos in quantum field theories, where the S-matrix is the ultimate observable. Although the chaos in scattering processes is fairly well understood both in classical mechanics [7, 8, 9] and in corresponding quantum/mechanical systems [10, 11], it is far from clear how the chaotic behavior manifests in quantum field theories. From what we know for first-quantized classically chaotic systems, one might expect that the eigenphases of the S-matrix can be characterized either by the *random matrix theory* (RMT) statistics, or by large and abrupt changes in the amplitude due to small changes in the kinematics (e.g. energy or the incoming angle)[Rosenhaus]. The same would be expected to occur in strongly coupled field theories, but analyzing such behavior in systems with many degrees of freedom makes the analytical investigation of chaos in quantum field theories a formidable task.

String theory, an eminent candidate for the theory of quantum gravity, provides numerous insights about black holes and gravity in general. One of them is the *black hole/string correspondence*, as proposed by Susskind [12] and developed by [13, 14], also-called the *Horowitz - Polchinski correspondence principle*. The correspondence suggests that a string excited to a sufficiently high level/occupation number is effectively described by a (semi-classical) black hole. This correspondence provides a way of studying black holes through the physics of highly excited strings (HES). The fact that the BH effective description should emerge at weak coupling, provides a rationale to look for the signs of chaos in the tree-level S-matrix of scattering processes including closed[2] HES states. Furthermore, from the QFT perspective, the scattering of the HES states involves exceedingly large number of degrees of freedom, making it possible to develop chaotic behavior even in the weak coupling limit. String theory thus enables us to explore both the BH chaos beyond the semi-classical regime and the chaos in QFT by studying the tree-level HES amplitudes for closed strings. Finally, most of the work done so far on string amplitudes has been focused on the amplitudes with low excitation numbers. The BH/string correspondence however hints at the rich structure of the HES amplitudes, making their investigation interesting also on its own.

The structure of the thesis is as follows: after shortly discussing the motivation and context of our work, we introduce the BH/string correspondence in some more detail in Section 1.1, then we provide a brief introduction to chaos with the focus on chaotic

[2]Gravitons appear in the spectrum of closed strings, and having in mind that the classical black hole is a bound coherent state of gravitons, we expect the BH/string correspondence to apply for the closed HES.

scattering in Section 1.2, and finish the Introduction by summarising the current state of the literature on HES scattering in Section 1.3. Then, in Chapter 2 we consider the classical scattering of the string off the black hole, which is valuable for comparison with the quantum case. Afterwards, in Chapter 3, we calculate the scattering amplitude of a HES state, first for an open string in Section 3.1, then in Section 3.2 we extend the result to the closed string using the KLT relations. In Section 3.3 we discuss the useful DDF formalism that we employ to describe the statistical properties of partitions for an arbitrary HES state in Section 3.4. The key results on the S-matrix phenomenology and the analysis of chaos are presented in Chapter 4, first for open strings (Section 4.1) and then for closed strings (Section 4.2). Finally, in Chapter 5 we summarise our results and conclusions and comment on possible directions of improving and extending our analysis.

Conventions: we use the mostly plus $(-,+,\ldots,+)$ signature and work in $c = \hbar = k_b = 1$ units. Except for the Section 1.1, we also set the string tension to $\alpha'/2 = 1$.

1.1 BH/string correspondence

Let us now motivate the BH/string correspondence, which states that a highly excited string should describe a black hole in the weak coupling regime. The idea stems from the fact that at sufficiently high occupation numbers, the Schwarzschild radius of the HES becomes smaller than the string scale, hence the string should collapse into BH. In the following we sum up the arguments from [12, 13, 14].

To make the argument qualitative, let us estimate both the string and the BH parameters. The mass of a string M_s and the mass of a black hole $M_{\rm BH}$ in $d+1$ spacetime dimension are

$$M_{\rm BH} \sim \frac{r_s^{d-2}}{G}, \;\; M_s \sim \frac{N}{\alpha'}, \tag{1.2}$$

where α' is the string tension, G is the Newton's constant and N the occupation number (level). At the string/BH transition, we expect the string length scale to be $\ell_s = \sqrt{\alpha'} \sim r_s$; then a string of mass M_s can become a black hole of mass $M_{\rm BH} = M_s \equiv M$. Thus we have two conditions (the equality of masses and length scales):

$$M^2 \sim \frac{N}{\alpha'} = \frac{(\alpha')^{d-2}}{G^2} \tag{1.3}$$

Equating the two sides and taking into account that $G \sim g^2\alpha'$ where g is the string coupling, we obtain the condition for the BH description of the string:

$$N g^4 \sim (\alpha')^{d-3} \Rightarrow g_c \propto N^{-1/4}(\alpha')^{d-3} \tag{1.4}$$

Therefore, to achieve the BH description at fixed α', we can either increase the coupling g (and decrease N), or the occupation number N (and decrease g). In the latter case the system can be described analytically in terms of a perturbative expansion in the coupling constant at the cost of going to large occupation numbers, at least around $N_c \sim 1/g^4$. In the former case the states are simple but the system becomes strongly coupled, making it inacessible to analytical considerations. Alternatively, in $d \neq 3$ we may vary α' at given N and g. Then we would need to include the string loops but without going to highly excited string states.

It is also instructive to take a look at the opposite process: if we start at weak coupling g, and increase it at fixed N and α', at some point r_s becomes smaller than the string size

so the metric near horizon is no longer well-defined, making the effective BH description inapplicable.

One can use this principle to compare the entropies of a BH and a HES. The well-known Bekenstein-Hawking area law gives $S_{\rm BH} \propto A \propto r_s^2 \propto (GM_{\rm BH})^2$. On the other hand, to estimate the HES entropy, we count the number of its states which is given by the number of partitions at the level N. The approximation of the number of partitions for large N gives $p(n) = \frac{1}{4\pi N} e^{\pi\sqrt{\frac{2N}{3}}}$ [15], yielding $S_{\rm HES} \propto \sqrt{N} \propto M_{\rm HES}$. This apparent disagreement of the entropy values is resolved by the fact that transition happens at a particular value of the coupling $g_c^4 \propto \frac{1}{N}$, hence $S_{\rm BH} \propto N$. Thus the BH/string correspondence implies that at the transition, the entropies of HES and black hole are equal up to possible factors of order unity.

1.2 Chaotic scattering

1.2.1 Basic phenomenology of chaos

The concept of chaos dates from the dawn of XX century, notably from the works of Henri Poincare and Aleksandr Mikhailovich Lyapunov, who studied the three-body problem, inspired by the question of the stability of the Solar system. Later it became clear that even incredibly simple systems can exhibit chaotic behavior. The basic idea behind the notion of chaos is that evolution of the system is highly sensitive to initial conditions. This corresponds to the exponential divergence of the two initially close orbits in the phase space:

$$|\vec{x}_1(t) - \vec{x}_2(t)| \propto e^{\lambda t}, \tag{1.5}$$

where the rate of the divergence λ is called the Lyapunov exponent. Although such local exponential divergence of the orbits is a necessary condition for chaos, there are systems which exhibit the behavior (1.5) in the vicinity of so-called hyperbolic points but are not chaotic, an example being the motion of the inverse harmonic oscillator.

If the system has a bounded phase space, then the exponential divergence, giving rise to the local stretch of the phase space must be followed by the folding of the phase space in order to preserve its volume (Liouville theorem). This combination of stretching and folding is the typical mechanism responsible for the chaotic dynamics of the closed systems. One of the simplest (and yet quite illustrative) examples of such dynamics is the baker's map on the unit square given by:

$$(x_{n+1}, y_n) = \left\{ \begin{array}{ll} (2x_n, \frac{y_n}{2}), & \text{if } 0 \le x_n \le \frac{1}{2} \\ (2x_n - 1, \frac{y_n+1}{2}), & \text{if } \frac{1}{2} \le x_n \le 1 \end{array} \right\} \tag{1.6}$$

which is essentially just the stretching of the left half of the square to match the bottom half, followed by stretching the right half to cover the upper half of the square. If one writes the coordinates in the square as $x = \sum_{n=1}^{\infty} \frac{c_{-n}}{2^n}, y = \sum_{n=0}^{\infty} \frac{c_n}{2^n}$ where $c_n \in \{0, 1\}$, one can represent the point by a bi-infinite sequence of characters $\ldots c_{-2}c_{-1}c_0c_1c_2\ldots$ often called 'word'. Then one can easily verify that applying the baker's map p times is equivalent to the transformation $c_n^{\rm old} \to c_n^{\rm new} = c_{n+p}^{\rm old}$ which is a simple leftward shift by p characters in the given word. Hence the baker's map is completely equivalent to the so-called shift dynamics of the bi-infinite word. From this point the sensitivity to the initial conditions is manifest: $c_{|n|}$ in the initial condition has a $\frac{1}{2^{|n|}}$ contribution in specifying the

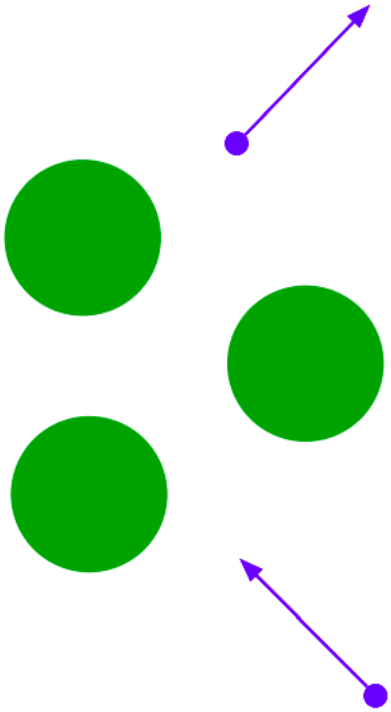

Figure 1.1: The stereotypical example of classical chaotic scattering: three hard planar disks on fixed positions in the plane provide a scattering potential for an incoming test particle. Depending on its incoming angle and velocity, the test particle will bounce off the disks a number of times (for periodic orbits the number is infinite) before continuing to infinity. Both the number of bounces and the scattering angle of the outgoing orbit depend sensitively on the incoming parameters, which encapsulates the idea of chaos. Unlike systems with finite phase space however, the total volume in any finite part of phase space is not preserved because of escaping orbits.

initial y coordinate, but after n steps it gives an estimate of the y coordinate within a $O(1)$ interval.

1.2.2 Chaos in classical scattering

The example from the previous subsection is typical in that the phase space is compact, so the textbook stretching and folding mechanism is the main motor of chaos. In scattering processes, on the other hand, the phase space is infinite. A typical setting for chaotic scattering is the scattering of a test particle off three non-collinear hard disks in the plane (Fig. 1.1).

One can specify the positions of the disks and scatter the particle off the disks with impact parameter b. Upon specifying the incoming state one can find the scattering angle θ which corresponds to the outgoing state. The sensitivity in the initial conditions is now contained in the $\theta(b)$ dependence. The function $\theta(b)$ does not merely look erratic (complicated), it admits a fractal structure; in other words the sensitivity is present at progressively smaller scales [7]. Such abrupt changes in the outgoing state for small changes in the incoming state correspond to the orbits in which the test particle bounces

off the disks many times before leaving to infinity. Obviously, trajectories with n and $n+1$ bounces have completely different outgoing states. the sensitivity to initial conditions generally increases with n. This hints that chaotic behavior stems from the set of unstable periodic orbits. Having that in mind, one can construct an array of numbers from the set $\{1, 2, 3\}$ describing the orbit, where the numbers label the disks which the particle hits on its trajectory. Such description of the orbit is again called symbolic dynamics [7, 8, 9], similar to the case of baker's map. The difference is that now the symbolic dynamics does not contain all the information about the orbit because it does not describe the escaping orbits; nevertheless, this 'coarse-grained' description captures the sets of long orbits which is essential for understanding the statistical properties of the dynamics, and thus can be used to calculate various diagnostics of chaos which are topological in nature, like the topological entropy.

1.2.3 Chaos and quantum mechanics

While the first hint of chaos in quantum mechanics is found in the pioneering paper by Einstein in 1917 [16], systematic study of so-called quantum chaos has started much later, in the framework of nuclear models [17]. In quantum mechanical systems, there is no exponential sensitivity to the initial conditions because the unitary evolution of the wavefunction is linear. Hence what is reasonable to ask is if there is some difference between the systems whose classical limit is chaotic and those whose classical limit is regular, or alternatively is there a useful notion of chaos in the semi-classical limit.

For a quantum scattering process, the fundamental observable is the S-matrix. In analogy with the erratic behavior of the scattering angle $\theta(b)$ in the classical scattering, the S-matrix for collisions at fixed energy changes abruptly with the change of the incoming or outgoing state. These strong fluctuations indicate that the system should be well-described by the Random Matrix Theory (RMT).

The RMT provides a statistical description of an ensemble of matrices whose elements are random variables with a specified distribution. The idea to describe the quantum mechanics of classically chaotic systems by RMT is the central tenet of quantum chaos studies [18, 17] and comes originally from studying the resonances of the nuclear decays. Bound states in nuclear physics typically represent a many-body system whose strongly coupled nature provides a rationale to model its Hamiltonian as a Hermitian matrix with random elements. Especially important is the Gaussian unitary random ensemble where the probability distribution of individual matrix elements is Gaussian with the overall constraint that the trace of the matrix is fixed, which effectively introduces correlations among the elements and eigenvalues of the matrix, leading to the celebrated effect of level repulsion, typical for quantum-chaotic Hamiltonians. If the system admits some kind of symmetry, this provides an additional constraint on the matrix elements besides hermiticity and changes the eigenvalue statistics. Wigner and Dyson have considered the time-reversal symmetry (TRS) and showed that it gives rise to three classes:

1. Systems with integer spin particles with TRS, whose Hamiltonian is a real matrix and hence orthogonal, are described by the Gaussian orthogonal ensemble (GOE).

2. Systems with half-integer spin particles with TRS are described by the Gaussian symplectic ensemble (GSE).

3. Systems without TRS are described by the Gaussian unitary ensemble (GUE).

These three ensembles predict the so-called Wigner-Dyson distribution for the eigenvalue spacings:

$$P(s) = A(\beta)s^{\beta}e^{-B(\beta)s^2} \tag{1.7}$$

where s is the level spacing divided by the average spacing value and β is the parameter specifying the TRS class:

$$\beta = \left\{ \begin{array}{ll} 1, & \text{integer spin with TRS (GOE)} \\ 2 & \text{no TRS (GUE)} \\ 4, & \text{half-integer spin with TRS (GSE)} \end{array} \right\} \tag{1.8}$$

The constants $A(\beta) = 2B(\beta)^{\frac{\beta}{2}+1}\Gamma(\frac{\beta}{2}+1)$ and $B(\beta) = \left(\frac{\Gamma(\frac{\beta}{2}+1)}{\Gamma(\frac{\beta+1}{2})}\right)^2$ are obtained from the normalization conditions $\int_0^1 P(s)ds = 1$ and $\int_0^1 sP(s)ds = 1$.

As pointed out in the work of Altland and Zirnbauer [19] in superconducting systems there is another discrete anti-unitary symmetry – charge conjugation which exchanges holes and particles. Together with the TRS, this provides ten classes of Gaussian ensembles, with are enumerated by compact symmetric spaces in modern literature [20].

The common property of all ten distributions is that the probability of zero spacing is suppressed, which is a consequence of the level repulsion. This is in contrast with the systems which are classically integrable, and nearly always admit Poisson distribution of the level spacings [17]. This can be understood from the point of degeneracy. Integrable systems generally admit more symmetries and hence their spectra tend to be degenerate. For a strongly coupled many-body system we generically do not expect any additional symmetries apart from TRS and possibly charge conjugation, therefore interactions break degeneracy and energy levels avoid each other.

As the RMT analysis is usually discussed (and was originally constructed) in the context of systems with bounded phase space, resulting in discrete energy spectrum, it is worth commenting on how the analysis works for scattering. The basic idea is that the S-matrix operator is essentially the evolution operator $S \sim e^{-iHt}$ with H being the Hamiltonian, so we can connect the energies to the eigenphases φ_i of the S - matrix $\epsilon \mapsto -\varphi$. Therefore, one should find the eigenvalues of the S-matrix and consider the *spacings between the phases of neighboring eigenvalues*, which should be described by the Wigner-Dyson distribution. For further details the reader may consult e.g. the review [10, 11].

Bearing these ideas in mind, one would generically expect the S-matrix to be an erratic function of incoming and outgoing states, and its eigenphases to follow the RMT predictions.

1.3 Chaos in string scattering

The study of chaos in string theory has been initiated fairly recently, in [21], where the authors introduce the highly excited string as a natural candidate for the analysis of chaos and lay out the roadmap of studying the statistics of their scattering amplitudes as a diagnostic of chaotic behavior (with some inspiration from the S-matrix in quantum field theory discussed in [22]). In [21, 23] a detailed analysis of a HES decaying into tachyons and photons is given. In [24] it is shown that the stst channel of this decay shows a complex and erratic structure as a function of the scattering angle – the first indication of quantum

chaotic scattering for strings. This was further corroborated in [25, 26, 27] where it is shown that the distribution of poles in the scattering amplitude (again in a single channel) is well-described by random matrix theory if the occupation numbers and the kinematics are chosen appropriately. In particular, [26] find that in the process where a HES decays to a tachyon and another HES, the positions of the peaks can be fit to a Wigner-Dyson distribution with the symmetry exponent being a free (fitting) parameter. Importantly, the authors find that HES states with many excited modes, which correspond to classical strings with complex and "wiggled" shapes, are in better agreement with a Gaussian random ensemble, as opposed to the states with only a few modes excited. Interestingly, in [27], it is found that for very higlyh excited levels, the symmetry exponent does not correspond to the expected value (2) for a time-reversal-invariant process – an inspiring puzzle for further work.

Finally, the work of Hashimoto, Matsuo and Yoda [28] is the first to consider in detail not just HES decay but the four-legged scattering process (of the form HES + t $\longrightarrow$ HES$'$ + t$'$ $\longrightarrow$, where HES, HES$'$ are highly excited strings and t, t$'$ are tachyons, i.e. ground states). For this process the authors do not find chaos (at least for small partitions and modest excitations levels) although they do find complex structures in the amplitude. This work has inspired us to look at the whole S-matrix for the same process, in order to uncover why the expected chaotic scattering is not there (it turns out it is present, but not equally in all channels, also mixed with regular dynamics, and limited to only certain partitions and incoming momenta, thus it may not be obvious at first glance).

So far all work on the dynamics of highly excited strings was done for open string amplitudes. Generalization to closed string HES is in principle straightforward as shown, e.g. in [29]: the same formalism which is employed in [21] to construct an arbitrary open HES vertex operator can be used also for closed string vertices. Numerically however closed strings are much more demanding as the state space is much larger. Nevertheless, one of the motives for our study was also to consider the dynamics of closed strings – closed strings contain graviton excitations and are thus more relevant for comparison with black holes.

Chapter 2

Chaos in classical string scattering

As a warmup and also to better understand the relation of the HES scattering to the classical black hole limit, we first consider the classical scattering of a closed string off the Schwarzschild black hole. We focus on the axially symmetric setup of [30], where the closed circle-shaped string is allowed to uniformly shrink and expand in its plane and move in the direction normal to itself (Fig. 2.1). A similar setup, so-called ring string, has been studied in a number of other contexts, e.g. gauge/string correspondence [31], (non)integrability [32] and chaos, both in string theory [33, 34, 35, 36, 37, 38] and in field theory [39].

We neglect the backreaction to the metric so that we have a motion of the test string in the fixed background. The Polyakov action $S_{\rm P}$ of the string in an arbitrary background metric reads

$$S_{\rm P} = \int d\tau d\sigma g_{\mu\nu}\eta^{ab}\partial_a X^\mu \partial_b X^\nu \tag{2.1}$$

where τ is the imelike and σ the spacelike coordinate of the worldsheet, $X^\mu(\tau,\sigma)$ is the string position, $a,b \in \{\tau,\sigma\}$ and $g_{\mu\nu}$ is the background metric. For an asymptotically planar Schwarzschild BH of mass M the metric is given by:

$$ds^2 = g_{\mu\nu}dx^\mu dx^\nu = -\left(1-\frac{2M}{r}\right)dt^2 + \frac{dr^2}{1-\frac{2M}{r}} + r^2 d\theta^2 + r^2\sin^2\theta d\phi^2 \tag{2.2}$$

in the usual Schwarzschild coordinates. By varying the action above one can obtain the equations of motion and the constraint equation for the string. Now the string configuration described above is described by the ansatz

$$t = t(\tau), r = r(\tau), \theta = \theta(\tau), \phi = \sigma. \tag{2.3}$$

The equations of motion reduce to a system of coupled ordinary differential equations (indeed, the appeal of this rather special and highly symmetric configuration is precisely that one can avoid solving partial differential equations):

$$\dot{t} = \frac{E}{1-\frac{2M}{r}}, \tag{2.4}$$

$$\ddot{r} = (r-3M)\dot{\theta}^2 - (r-M)\sin^2\theta, \tag{2.5}$$

$$\ddot{\theta} = -\frac{2}{r}\dot{\theta}\dot{r} - \sin\theta\cos\theta. \tag{2.6}$$

The first equation is simply a consequence of the time translation invariance, that is existence of the timelike Killing vector, and E is the corresponding integral of motion,

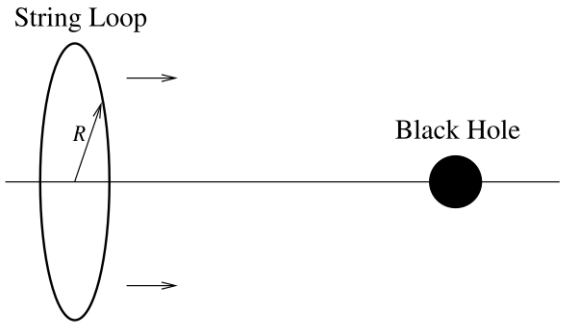

Figure 2.1: Geometry and kinematics of the closed string-black hole scattering process as first considered in [30]. A circular string of radius RR which winds in the $x - y$ plane approaches the black hole along the z-axis, staying parallel to itself. The string may bounce backwards, pass the black hole and continue forward, or be captured and fall into the black hole. This setup shows classical chaotic scattering. Adopted from [30].

with the meaning of energy. The equations of motion (2.4-2.6) are supplemented by the constraint

$$\dot{r}^2 + (r^2 - 2Mr)(\dot{\theta}^2 + \sin^2\theta) = E^2. \tag{2.7}$$

One can investigate the dynamics of this string configuration by solving the equations (2.4-2.7) numerically. Clearly, there are only three possible asymptotic states: forward scattering where the string escapes to $+\infty$, backscattering, when the string bounces and returns to $-\infty$, and the collapse of the string into the BH.

Solving the above equations numerically,[1] we find strong sensitivity of the future asymptotic state on the initial conditions, the expected sign of chaos, as the system is nonintegrable (E being the only integral of motion). This is illustrated in Fig. 2.2.

In the work of Frolov and Larsen it was shown that as one increases E through $E \approx 5.67M$, dynamics abruptly changes from regular to chaotic. The existence of minimal E is not surprising, because at low energies string just falls into the BH, while for higher energies it can shrink multiple times before it skips over the back hole. In the chaotic regime, they find the fractal set of unstable orbits (strange repeller).

A more thorough investigation of chaos in the dynamics of closed strings in the background of an AdS black hole, discussing the extension of Eq. (1.1) to strings with higher winding numbers can be found in [40].

[1] We integrate the system of (2.5) and (2.6) to find $r(\tau)$ and $\theta(\tau)$ using the Mathematica NDSolve command. Then we check that the constraint 2.7 is satisfied (within the numerical precision) on the solutions we find, and finally integrate (2.4) to find $t(\tau)$.

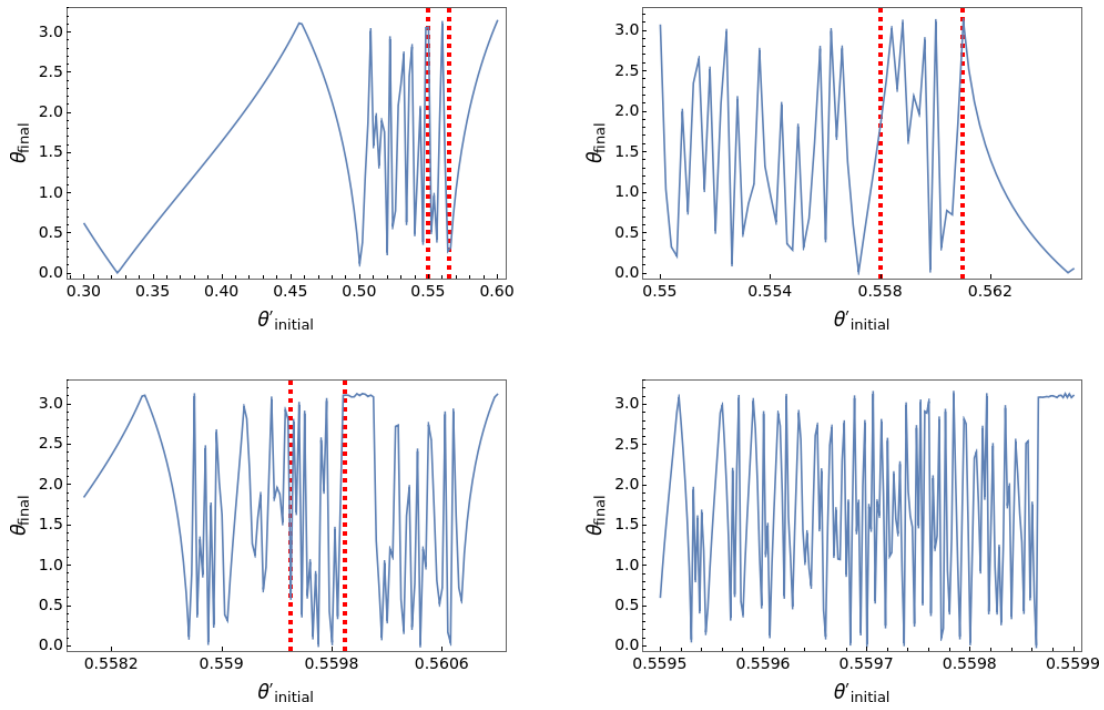

Figure 2.2: Highly sensitive dependence of the final scattering angle θ_{final} on the derivative of the angle with respect to proper time τ at initial time $\dot{\theta}_{\text{initial}}$ for $r_{\text{initial}} = 10$, $\dot{r}_{\text{initial}} = 0.2$ and $\theta_{\text{initial}} = \arcsin(0.3)$. As we zoom in to smaller and smaller intervals (labeled by red dashed lines in each subplot), we observe persistently complex dependence, as expected for a chaotic system.

Chapter 3

Quantum scattering of highly excited strings

In this chapter we start the study of the main topic of this thesis, quantum scattering of highly excited bosonic strings. We discuss tree-level scattering of two HES states, denoted by HES and HES$'$, and two tachyon states, t and t$'$:

$$\text{HES} + \text{t} \longrightarrow \text{HES}' + \text{t}'. \tag{3.1}$$

In the first section we follow the formalism of [28] for open strings, and then we exploit the KLT relations [41, 42, 43] to construct the analogous amplitude for closed strings.

3.1 Open string amplitudes

The HES represent the state with a large number of excitations $\{n_k\}$, or equivalently on a high level $N = \sum_k k n_k$, where k labels the modes and n_k is the occupation number of the k-th mode. In the lightcone quantization the general HES state has the form [29]:

$$|\text{HES}\rangle \propto \xi^{i_1 \dots i_J} P\left(\partial X, \dots \partial^N X\right)_{i_1 \dots i_J} |0, p\rangle \tag{3.2}$$

where $\xi^{i_1 \dots i_J}$ is the polarization tensor, P is a polynomial over the derivatives of the string coordinates X^μ and $|0, p\rangle$ is the tachyon state (ground state of the bosonic string) with momentum p. Following the DDF formalism [44, 29, 45], a convenient way to think of the HES state is as a state created in a process in which the tachyon (the state with no excitations) absorbs J photons with momenta q_i and polarizations λ_i one by one (FIG). Hence, we extract the sought for amplitude by first considering the amplitude for the process

$$\text{tachyon}(1) + (\text{tachyon}(2) + J \text{ photons}) + \text{tachyon}(1') + (\text{tachyon}(2') + J' \text{ photons}), \tag{3.3}$$

and then picking out the poles so that the (tachyon + # photons) part of the amplitude creates an intermediate on-shell HES state 3.1.

For this procedure to describe the absorption of # photons by the tachyon one by one, it is necessary to remove the terms which couple photons to each other. These are proportional to $\lambda_i \cdot \lambda_j$, so we must take the polarizations of different photons to be orthogonal to each other. For the sake of simplicity, we achieve this simply by choosing $\lambda_i \equiv \lambda$ such that $\lambda \cdot \lambda = 0$ and $q_a = -N_a q$ where N_a is a positive integer and q satisfies

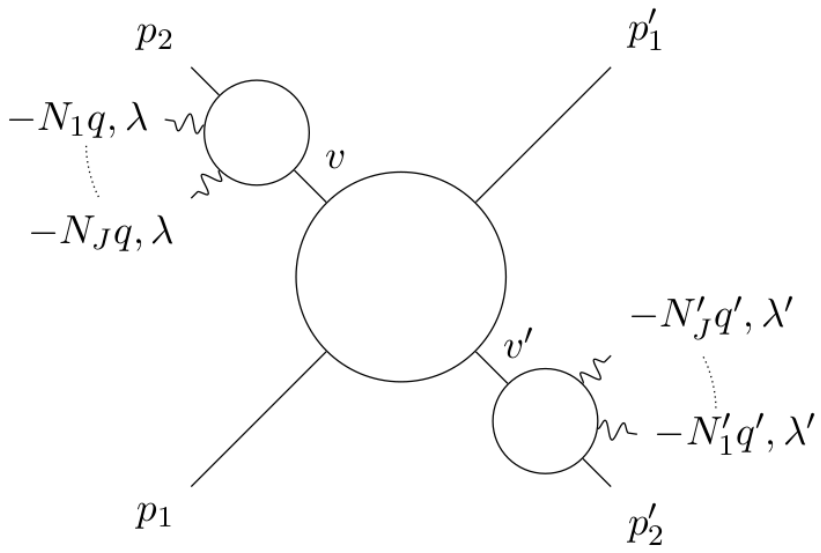

Figure 3.1: String amplitude for the HES-tachyon scattering process (3.1). The tachyon labeled by its momentum p_2 absorbs J photons with momenta and polarizations $\{-N_k q, \lambda\}$ which (after picking out appropriate poles) results in a HES state labeled by v (similarly for the HES$'$). The two HES states interact with tachyons labeled by p_1 and p_1'. Adapted from [28].

the condition $q \cdot \lambda = 0$ (the essentially states that all polarizations are transverse, as they have to be for photons). For the HES$'$ state we similarly take $\lambda' \cdot \lambda' = 0$ and $q_b' = -N_b' q'$. To find the tree-level amplitude we use the tachyon vertex operator $: V_t(z,p) =: e^{ipX(z)} :$, employ a computational trick to replace the photon vertex operators by $: e^{i\zeta \partial X + ikX} :$ and keep only the part linear in the polarization ζ.

When the HES state is constructed as described above, we can express the tree-level amplitude as the path integral over the product of the vertex operators:

$$\mathcal{A} = \frac{1}{\mathrm{Vol}\,(\mathrm{SL}\,(2,\mathbb{R}))} \int \mathcal{D}X e^{-S_\mathrm{P}} \int \prod_i dw_i V_t(w_i, p_i) \prod_a dz_a V_p(z_a, -N_a q, \lambda) \prod_b dz_b' V_p(z_b', -N_b' q, \lambda) \tag{3.4}$$

where $i \in \{1, 2, 1', 2'\}$ runs over the tachyons, $a \in \{1, \ldots, J\}$ runs over the photons in HES, $b \in \{1, \ldots, J'\}$ runs over the photons in HES$'$ and the integration variables z and w run over the worldsheet. The action in the path integral is the usual Polyakov action $S_\mathrm{P} = -\frac{1}{4\pi\alpha'} \int_z dz (\partial X)^2$. Next, we choose $\lambda' \propto \lambda$ and $q' \propto q$ to simplify the calculation and perform the contractions to obtain:

$$\begin{aligned} \mathcal{A} \;&=\; \frac{1}{\mathrm{Vol}\,(\mathrm{SL}\,(2,\mathbb{R}))} \int_{-\infty}^{\infty} \prod_i dw_i \int_{-\infty}^{\infty} \prod_a^J dz_a \int_{-\infty}^{\infty} \prod_b^{J'} dz_b' \times \\ &\times\; \prod_{i<j} |w_i - w_j|^{p_i \cdot p_j} \prod_{a,i} |z_a - w_i|^{-\alpha_i} \sum_i \frac{-p_i \cdot \lambda}{w_i - z_a} \prod_{b,j} |z_b' - w_j|^{-\beta_j} \sum_j \frac{-p_j \cdot \lambda'}{w_j - z_b'} \end{aligned} \tag{3.5}$$

where we have expanded the integrand to the linear order in photon polarizations, and introduced $\alpha_i = N_a p_i \cdot q$ and $\beta_j = N_b' p_j \cdot q'$. After exploiting the residual $\mathrm{SL}(2,\mathbb{R})$ gauge invariance of the worldsheet to fix three out of four w_i values, we end up with the following

six channels of the amplitude:

$$\mathcal{A} = \mathcal{A}_{st} + \mathcal{A}_{tu} + \mathcal{A}_{us} + \mathcal{A}_{ts} + \mathcal{A}_{ut} + \mathcal{A}_{su}. \tag{3.6}$$

It is enough to state in full the expression for one channel; the others are then obtained by simple replacement of the momenta. We give the expression for the *st* channel:

$$\mathcal{A}_{st} = \mathcal{A}|_{w_1'=-\infty,w_2=0,w_1=w,w_2'=1} = \int_0^1 dw w^{p_1\cdot p_2}(1-w)^{p_1\cdot p_2'} \prod_{a=1}^{J} Z_a^{212'}(\alpha,p,\lambda;w) \prod_{b=1}^{J'} Z_b^{212'}(\beta,p,\lambda';w), \tag{3.7}$$

where we have defined the integral

$$Z_a^{ijk}(\alpha,p,\lambda;w) = \int_{-\infty}^{\infty} dz_a |z_a|^{-\alpha_i} |z_a - w|^{-\alpha_j} |z_a - 1|^{-\alpha_k} \left(\frac{-p_i\cdot\lambda}{-z_a} + \frac{-p_j\cdot\lambda}{w-z_a} + \frac{-p_k\cdot\lambda}{1-z_a} \right). \tag{3.8}$$

The other channels are now related to the stst channel in the following way:

$$\begin{aligned}
\mathcal{A}_{tu} &= \mathcal{A}|_{w_2=-\infty,w_2'=0,w_1=w,w_1'=1} = \mathcal{A}_{st}|_{2\to 2',2'\to 1'}, && (3.9)\\
\mathcal{A}_{us} &= \mathcal{A}|_{w_2'=-\infty,w_1'=0,w_1=w,w_2=1} = \mathcal{A}_{st}|_{2\to 1',2'\to 2}, && (3.10)\\
\mathcal{A}_{ts} &= \mathcal{A}_{st}|_{2\longleftrightarrow 2'}, && (3.11)\\
\mathcal{A}_{ut} &= \mathcal{A}_{tu}|_{2'\longleftrightarrow 1'}, && (3.12)\\
\mathcal{A}_{su} &= \mathcal{A}_{us}|_{1'\longleftrightarrow 2}, && (3.13)\\
& && (3.14)
\end{aligned}$$

The on-shell condition needed to create HES and HES′ is that after the first $j \le J$ photons have been absorbed, the mass of the intermediate state is $M_j = 2(\sum_{a\le j} N_a - 1)$. Having in mind that the total momentum of this intermediate state is $p_2 - \sum_{a\le j} q$, and using the on-shell condition for tachyons $-p_2^2 = -2$, we obtain:

$$\alpha_2 \to N_a, \beta_2' \to N_b' \tag{3.15}$$

where the second condition comes from HES′. The Z_a^{ijk} integrals can be written in terms of the regularized hypergeometric function, whose Taylor series admit coefficients containing the combination of Γ functions. This calculation is thoroughly described in [28], the result for the *st* channel being

$$\mathcal{A}_{st} = \sum_{\{i_a\in\{2,2'\}\}} \sum_{\{j_b\in\{2,2'\}\}} \sum_{\{k_a=1\}}^{\{N_a\}} \sum_{\{l_b=1\}}^{\{N_b'\}} \left(\prod_a^J (p_{i_a}\cdot\lambda) c_{k_a}^{(i_a)} \right) \left(\prod_b^{J'} (p_{j_b}\cdot\lambda') d_{l_b}^{(j_b)} \right) B\left(-1-\frac{s}{2}+k, -1-\frac{t}{2}+l\right) \tag{3.16}$$

where $l = \sum_b^{J'} l_b$, $k = \sum_a^J k_a$ and the coefficients c and d are defined as:

$$\begin{aligned}
c_k^{(2)} &= c_k(\alpha_2+1, \alpha_1+1, \alpha_2'), && (3.17)\\
c_k^{(2')} &= -c_{k-1}(\alpha_2, \alpha_1, \alpha_2'+1), && (3.18)\\
d_l^{(2)} &= -c_{l-1}(\beta_2', \beta_1, \beta_2+1), && (3.19)\\
d_l^{(2')} &= c_l(\beta_2'+1, \beta_1+1, \beta_2), && (3.20)\\
& && (3.21)
\end{aligned}$$

using the function:

$$c_k(\alpha_2, \alpha_1, \alpha_2') = \frac{\pi}{\sin \pi\alpha_2} \frac{\Gamma(\alpha_2 - k + \alpha_1 - 1)\Gamma(\alpha_2' + k)}{\Gamma(\alpha_1)\Gamma(\alpha_2')\Gamma(\alpha_2 - k)\Gamma(k+1)}, \tag{3.22}$$

and finally the beta function is defined as usual: $B(x,y) = \Gamma(x)\Gamma(y)/\Gamma(x+y)$.

Because of the condition 3.15 the c and d coefficients diverge due to the $\frac{\pi}{\sin \pi\alpha_2}$ factor in 3.22. This divergence is just the expected behavior of the amplitude when one of the internal momenta in the diagram are on-shell. In order to extract the sought amplitude of the HES + t $\longrightarrow$ HES$'$ + t$'$ process, besides the on-shell conditions 3.15, we have to regularize amplitude.[1] To achieve this we simply ommit the divergent $\frac{\pi}{\sin \pi\alpha_2}$ part in the definition 3.22 in our calculations, resulting in finite expression for the sought amplitude (except of course for the special choices of kinematics).

Note that for generic partition $\sum_{a=1}^{J} N_a = N$ the number of operations needed to compute the amplitude 3.16 increases rapidly with the partition lengths J and J' due to the increase in number of sums over k_a and l_b. In addition, the number of states with fixed level N grows exponentially in $\sqrt{N}$. These two effects make the calculation of the S-matrix elements in the whole subspace of N and fixed kinematics computationally demanding, heavily limiting the levels accessible for our considerations at the level of the S-matrix. On the other hand, in a generic quantum field theory, the number of states does not increase with energy so rapidly, providing only a small (of order $O(1)$) number of channels through which chaos can develop. Hence one would expect chaos to emerge only at strong coupling. This implies that even though the large number of HES states makes the problem computationally demanding, it is also the reason why even strong chaos may be probed analytically (at least in principle) in the HES scattering.

3.1.1 Kinematics

Now we briefly discuss the kinematics we choose for calculation of the amplitude (following [28]). A look at the expression (3.16) for A_{st} tells that the kinematics is highly non-unique: there are many momenta and polarizations involved and we have many parameters to choose. We have made no attempt to consider their influence in detail. We have varied just a few quantities and they seem not to influence the dynamics in a qualitative way, except for the magnitude of the incoming momentum, which is quite crucial as we shall see. As noted above, p_1 and p_1' are the momenta of the on-shell tachyons and HES is created from the tachyons with momenta p_2, and a set of J photons with momenta $\{-N_a q\}$ whose polarizations are all equal to λ (similarly for the HES$'$ we have $p_2', J', \{N_b'\}, q'$ and λ'). The momentum conservation equation now reads:

$$p_1 + (p_2 - Nq) + p_1' + (p_2' - Nq') = 0 \tag{3.23}$$

The total mass of HES (and HES$'$) is given by the total occupation number $M = 2(N-1) = 2(N'-1)$, while J and J' represent the total spin of HES and HES$'$ respectively because the photons have identical polarizations. The tachyon momenta satisfy the on-shell condition $-p_i^2 = -\left(p_i'\right)^2 = -2$. We choose to work in the center-of-mass frame and, as we already mentioned, for simplicity we take the polarizations and photon momenta to

[1] This procedure is essentialy the same as in the QFT where one would remove the divergence by multiplying the amplitude by the inverse propagator of the internal on-shell particle

satisfy $\lambda = -\lambda'$, $\lambda \cdot \lambda = 0$ and $q' \propto q$. In order to satisfy these conditions we parametrize the momenta and the polarizations in the following way:

$$\begin{aligned}
q &= \frac{1}{\sqrt{2(N-1)+p^2} - p\cos\theta}(-1,0,0,1)^T \\
q' &= \frac{1}{\sqrt{2(N-1)+p^2} - p\cos\theta'}(1,0,0,-1)^T \\
p_1 &= (\sqrt{p^2-2}, p\sin\theta, 0, p\cos\theta)^T \\
p_1' &= -(\sqrt{p^2-2}, p\sin\theta'\cos\phi', \sin\theta'\sin\phi', p\cos\theta')^T \\
p_2 &= Nq - p_1 = (\sqrt{s},0,0,0)^T, p_2' = N'q' - p_1' - (\sqrt{s},0,0,0)^T \\
\lambda &= \frac{1}{\sqrt{2}}(0,1,i,0)^T,
\end{aligned} \tag{3.24}$$

and define Mandelstam-like variables:

$$s = -(p_1+p_2-Nq)^2 = \left(\sqrt{2(N-1)+p^2-2}+\sqrt{p^2-2}\right)^2 \tag{3.25}$$

$$\begin{aligned}
t &= -(p1+p_2'-N'q')^2 = \left(\sqrt{2(N-1)-p^2-2}+\sqrt{p^2-2}\right)^2 - \\
&\quad -2p^2\left(1+\cos\theta\cos\theta'+\sin\theta\sin\theta'\cos\phi'\right)
\end{aligned} \tag{3.26}$$

$$u = -(p_1+p_1')^2 = -2p^2\left(1-\cos\theta\cos\theta'-\sin\theta\sin\theta'\cos\phi'\right). \tag{3.27}$$

In this parametrization we obtain $p_2 \cdot q = p_2' \cdot q' = 1$ as required by the on-shell conditions (3.15) (e.g. $\alpha_2 = N_a p_2 \cdot q \to N_a$). Furthermore, the only imaginary contribution to $\mathcal{A}_{st}$ comes from the $(p \cdot \lambda)$ factors which we calculate to be $p_2' \cdot \lambda' = -\frac{\sin\theta' p}{\sqrt{2}} e^{i\phi'}$. Hence for $\phi' = 0$ we expect the amplitudes calculated from [3.16] to be real. For the collinear kinematics, that is $\theta, \theta' \in \{0, \pi\}$, the amplitude vanishes as can be seen from the fact that λ is orthogonal to all momenta. In general, the amplitude is fully characterized by the module of the momentum p, scattering angles θ, θ' and ϕ', and by the partitions of the levels N_a and N_b'. The amplitudes then define the elements of the S-matrix for fixed kinematics $(p, \theta, \theta', \phi')$ in the basis of different partitions of the level N.

3.2 Closed string amplitudes

In the previous section we have described the scattering of HES for open bosonic strings. While this process merits some interest on its own, if we want to make contact with black holes or the classical scattering setup from Chapter 2, we should consider closed string amplitudes. Although this can be achieved in a similar way as for the open case, making use of the DDF operators, at tree-level, we can circumvent this calculation by employing the celebrated KLT relations [41, 42, 43]. The idea behind the KLT relations is that a closed string amplitude can be constructed from two open string amplitudes coupled by the momentum-dependent kernel. This connection between the open and closed string tree-level amplitudes can be seen from the fact that the closed string propagator can be constructed by joining the two open string propagators. Schematically, an M-point closed string amplitude $\mathcal{A}^M_{\text{closed}}$ is given by:

$$\mathcal{A}^M_{\text{closed}} \propto \sum_{P,P'} \mathcal{A}(P)^M_{\text{open}} \bar{\mathcal{A}}(P')^M_{\text{open}} e^{iF(P,P')} \tag{3.28}$$

where P and P' denote the permutations of the M external legs, $\mathcal{A}(P)^M_{\text{open}}$ is the ordered M-point open string amplitude and F is a phase determined by the kinematics. In the field theory limit ($\alpha' \to 0$), for $M = 3$, one recovers that the three-point graviton vertex is equal to the product of the two color-stripped Yang-Mills three-point vertices, an example of the double copy relation between field theories [46].

In the case of interest for us, that is for the four-leg scattering, the KLT relation becomes particularly simple:

$$\zeta_{\mu_1\dots\mu_4,\nu_1,\dots\nu_4}\mathcal{A}^{\mu_1\dots\mu_4,\nu_1\dots\nu_4}_{\text{closed}} = -\pi\sin(\pi p_2\cdot p_1')\xi_{\mu_1\dots\mu_4}\mathcal{A}^{\mu_1\dots\mu_4}_{\text{open}}(s,t)\xi'_{\mu_1\dots\mu_4}\mathcal{A}'^{\nu_1\dots\nu_4}_{\text{open}}(t,u). \quad (3.29)$$

This enables us to construct the closed string S-matrix as a direct product of the *st* and tutu contributions to the open string S-matrix. If we consider fixed kinematics and vary the partitions, the direct product structure changes the dimensions of the S-matrix from $p(N)\times p(N)$ for open to $p(N)^2\times p(N)^2$ for closed strings, which is a big enhancement in size having in mind the fast growth of the number of partitions $p(N)$ with N.

3.3 The DDF formalism for HES vertex operators

So far we have managed to circumvent the problem of finding the HES vertex operator and we have found the amplitude for HES states for a special choice of polarizations (corresponding to our choice of $\lambda_a = \lambda = -\lambda'_b$ and $q_a = q \propto -q'_b$). In order to specify an arbitrary HES state, it would be useful to utilise a more systematic procedure. Here we shortly review the construction due to Del Giudice, Di Vecchia and Fubini (DDF) [44, 29, 45] which is inspired by the same physical idea of tachyon absorbing the photons that we have already used, enabling us to find a general HES vertex operator.

Essentially the problem boils down to finding the covariant vertex operator representing the arbitrary physical state of the string. Naively, one would freely combine creation operators $\dagger\,(\alpha^\mu_k)^\dagger$ for various modes k and their products, but this in general does not satisfy the Virasoro constraints. In order to make linear combinations which satisfy the constraints, one defines the DDF operators $A^i_n = \oint \frac{dz}{2\pi}\partial_z X^i(z)e^{inq\cdot X(z)}$ and calculate the vertex operator as a radially ordered product

$$V^{(r)}(w) = \xi_{i\dots j} : A^i_{-n_1}\dots A^j_{-n_r}e^{ip\cdot X(w)} :, \quad (3.30)$$

corresponding to the state with the level $\sum_i n_i = N$ and momentum $(p-Nq)^\mu$, with the on-shell condition $-(p-Nq)^2 = 2(N-1)$ satisfied provided that $p\cdot q = 1$. Due to radial ordering, the expression above actually resembles the process of tachyon with momentum p absorbing r photons of momenta $-n_i q$ (Eq. 3.2).

It is not hard to verify that the DDF operators may be interpreted as "creation operators" which are compatible with the Virasoro constraints. This, together with the one-to-one correspondence with the arbitrary state in the lightcone quantization $|V\rangle_{lc} = \xi_{i\dots j}\left(\alpha^i_{n_1}\right)^\dagger\dots\left(\alpha^j_{n_r}\right)^\dagger|0,p\rangle$, proves that the DDF operators are sufficient to construct the whole Fock space. Even though here we discussed the open string case, the formalism is easily generalised to closed strings by introducing another set of operators $\bar{A}^i_{\bar{n}} = \oint \frac{d\bar{z}}{2\pi}\partial_{\bar{z}}X^i(\bar{z})e^{i\bar{n}q\cdot X(\bar{z})}$ and replacing the open string tachyon vertex operator with the closed string version, taking care of the anti-holomorphic sector. In the closed string case the procedure is again sufficient to build the whole Fock space, provided the level matching condition $\bar{N} = \sum_i \bar{n}_i = \sum_i n_i = N$ is satisfied.

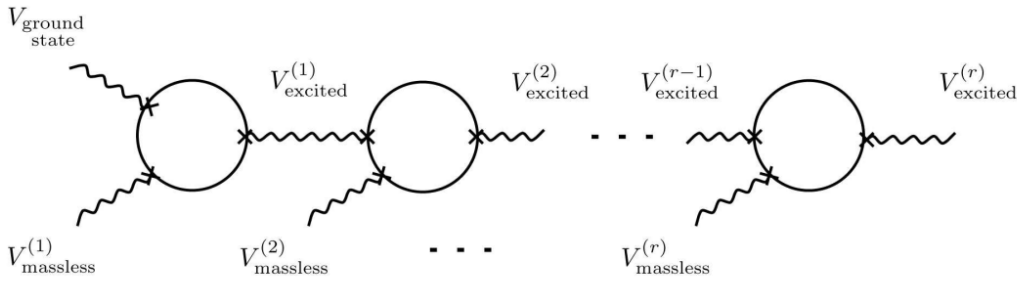

Figure 3.2: Illustration of the DDF procedure for obtaining an arbitrary physical open string vertex operator. The tachyon (labeled by $V_{\text{ground state}}$) absorbs the photons $V^{(k)}_{\text{massless}}$ one by one, resulting in intermediate excited states $V^{(k)}_{\text{excited}}$ $(k = 1, \dots r)$, yielding the $V^{(r)}_{\text{excited}}$ state in the end. Adapted from [29].

Thus the DDF construction can be used to construct an arbitrary HES state. But as already mentioned, [21] has found through the use of the DDF formalism that the contribution from non-orthogonal polarizations is suppressed for large N, and that the leading term is sufficient to provide a complex structure of the HES amplitudes. Hence we choose to analyse the HES amplitudes for the kinematics we have specified in subsection 3.1.1, Eqs. (3.24-3.27).

3.4 Statistics of the level partitions

Clearly, the number of partitions $p(N)$ has a very fast growth with N. In order to characterize the complexity of dynamics in the next chapter it is useful to consider the statistics of partitions in some more detail. We close this chapter on the HES amplitudes by finding the average occupation numbers of the given mode at level N.

Consider first the open string. We focus on $\langle n_k \rangle$, the average occupation of the mode k. Bearing in mind the physical interpretation of the DDF process of creating a HES from a multiple of photons, and interpreting $N = \sum_k k n_k$ as the total energy of the indistinguishable bosons, it is easy to answer this question. We can treat it in a grand canonical ensemble with zero chemical potential (because we work with photons):

$$Z = \sum_{\text{configurations}} e^{-\frac{E_{\text{tot}}}{T}} = \sum_{\{n_k\}} \prod_k C_k e^{-\frac{k n_k}{T}} = \prod_k Z_k \tag{3.31}$$

where C_k is the degeneracy of the mode k due to polarization choice, which reads $C_k = \binom{n_k+D-2-1}{n_k} = (-1)^{n_k}\binom{2-D}{n_k}$ in D spacetime dimensions, and T is the temperature. Also the fact that different modes do not interact allows us to define a grand partition function for a single mode:

$$Z_k = \sum_{n_k} C_k e^{-\frac{k n_k}{T}} = (1 - e^{-\frac{k}{T}})^{2-D}. \tag{3.32}$$

Plugging in the above result into (3.31) we can find the average occupation of the mode:

$$\langle n_k \rangle = -\frac{1}{k}\frac{\partial}{\partial T^{-1}} \log Z_k = \frac{D-2}{e^{\frac{k}{T}} - 1}, \tag{3.33}$$

which is the Bose-Einstein distribution as expected. The $D-2$ factor is simply due to the number of polarizations. In order to find T we should demand that the average of the total energy is equal to N. It is clear that the $N \gg 1$ corresponds to the high energy limit, or equivalently $\frac{1}{T} \ll 1$. In this limit we can analytically estimate Z:

$$Z = \prod_k Z_k = \exp\left\{(2-D)\sum_k \log\left(1-e^{-\frac{k}{T}}\right)\right\} \approx \exp\left\{(D-2)\sum_{k,n=1}^{\infty}\frac{e^{-\frac{kn}{T}}}{n}\right\}. \tag{3.34}$$

We can evaluate the sum in the exponent by expanding over $\frac{1}{T} \ll 1$:

$$\sum_{k,n=1}^{\infty}\frac{e^{-\frac{kn}{T}}}{n} = \sum_n \frac{1}{n}\frac{1}{e^{\frac{n}{T}}-1} \approx \sum_n \frac{T}{n^2} = \frac{\pi^2 T}{6}. \tag{3.35}$$

In the high energy limit we thus have $Z \approx e^{\frac{\pi^2(D-2)T}{6}}$, and using $\langle E\rangle = -\frac{\partial}{\partial T^{-1}}\log Z$ we find the inverse temperature $\frac{1}{T} = \pi\sqrt{\frac{D-2}{6N}}$.

We can easily generalize this to the closed string HES with $\sum_k n_k = \sum_k n_k' = N$. We find the grand partition function:

$$Z_{\text{closed}} = \sum_{\{n_k\},\{n_p'\}}\prod_{k,p} C_k C_p' e^{-\frac{\sum_{k,p}(kn_k+pn_p')}{T}} = Z_{\text{closed}}^2 \tag{3.36}$$

by using the fact that different modes do not interact neither inside nor outside of a given sector. Therefore, in the high energy limit we get simply

$$Z_{\text{closed}} = Z^2 = e^{\frac{\pi^2(D-2)T}{3}}. \tag{3.37}$$

From the level matching condition we have $\langle E\rangle = \sum_k k(n_k+n_k') = 2N$. Using this to find the inverse temperature we obtain $\frac{1}{T} = \pi\sqrt{\frac{(D-2)}{6N}}$ just as for open string HES. It is easy to show that we again have the Bose-Einstein distribution for the occupation numbers in both sectors.

Even though the average n_k for a fixed N is useful information, it probably does not say much about which modes are the most significant in dynamics and which could give rise to chaotic behavior. Bose-Einstein statistics implies that the most common excitations are those with $k \sim 1$, and the partitions containing only low k excitations will hardly contribute to chaos due to their simplicity. On the other hand, it was found [21] that in the large N limit, most of the contribution to N comes from the $k \sim \sqrt{N}$ modes, which at large N give rise to complex classical string configuration, and could hopefully drive the chaos [27], and possibly be significant for the dynamics (including S-matrix) at high energies.

In order to describe the complexity of dynamics, it is useful to introduce the Shannon information entropy $S_i = -\text{Tr}[\rho\log\rho]$. Based on the assumption that every state has *a priori* equal probability, the density matrix at temperature T has elements $\rho(\epsilon) \sim e^{-\frac{\epsilon}{T}}$. To calculate the entropy for the scattering process, we replace the energies ϵ_i by eigenphases ϕ_i of the S-matrix as discussed in subsection 1.2.3. Thus, we associate the entropy to the scattering process at fixed kinematics and level and calculate it as the sum over the eigenphases:

$$S_i = -\sum_{i=1}\varphi_i e^{\varphi_i}. \tag{3.38}$$

As the dynamics becomes chaotic, we expect the information entropy to increase, reflecting the increase in the dynamics complexity.

Chapter 4

Chaos in the quantum scattering of highly excited strings

In this chapter, we present and discuss our numerical investigation of the amplitudes involving HES states for the setting described in the previous chapter. We start by considering the phenomenology of the open string amplitudes and then move to discuss the physically more relevant closed string amplitudes.

4.1 Phenomenology of open string scattering

Here we present the results of the calculation of the closed S-matrix for the process (3.1) involving two HES states and the two tachyons. Because of the complexity of the expression (3.16) for $\mathcal{A}_{st}$ the computation time grows rapidly, limiting our considerations to $N \lesssim 10$.[1] We calculate the amplitudes for fixed kinematics and all possible partitions specifying the two HES states and from these we obtain the S-matrix on the subspace of fixed kinematics (which we call simply the S-matrix).

We diagonalize the S-matrix to obtain its basis-independent characteristics - the eigenvalues (the eigenphases are in particular relevant for RMT statistics) and eigenvectors. In order to see what kind of partitions dominates the dynamics, we plot the eigenvector corresponding to the eigenvalue with the largest absolute value for various momentum intensities p and angles θ, θ' and ϕ'. We characterize the contribution of different partitions to dynamics by magnitudes of the corresponding components of the highest eigenvector,[2] and by magnitudes of the S-matrix elements in the basis of states specified by partitions. We find that small partitions (the ones with small spin J) dominantly contribute to the highest eigenvector at small momenta p, while for large momenta long partitions dominate the highest eigenvector (Fig. 4.1). The crossover from the domination of small partitions to the domination of large partitions happens at the momentum value that we denote by p_c: at $p = p_c$ partitions of all lengths contribute equally. We find p_c slightly decreases with increasing ϕ'.

This can be roughly understood in a simple way: for $p \gtrsim p_c$ there is enough energy to activate most of the modes. The fact that at large energies large partitions dominantly

[1] In [24, 21, 26, 27] much larger N values were considered, however the calculations in these papers were performed for the three-leg and four-leg processes including one HES state, and only for a subset of amplitudes, allowing them to investigate higher levels.

[2] We order the eigenvectors by the size of their corresponding eigenvalues. The highest eigenvector is thus the eigenvector that corresponds to the largest eigenvalue.

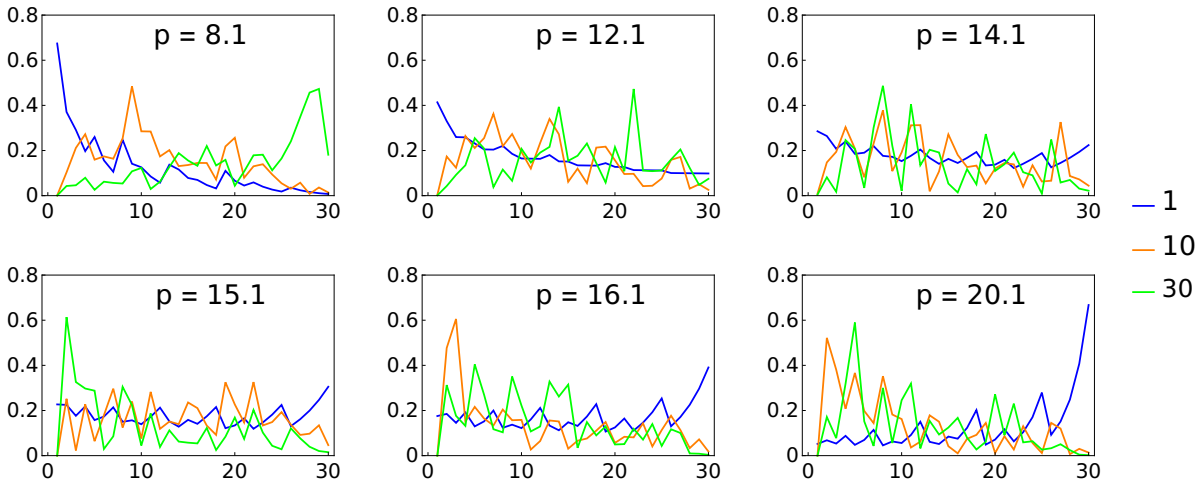

Figure 4.1: Coefficients of the S-matrix eigenvector no. n in the partition basis, for $n = 1, 10, 30$ (blue, orange, green) and six momentum values $p = 8.1, 12.1, 14.1, 15.1, 16.1, 20.1$ assuming $N = 9$, $\theta = 0.23$, $\theta' = 0.3$ and $\phi' = 0.7$. The partitions are numerated from shortest (of the form $(0, \dots 0, N, 0, \dots 0)$) to longest (of the form $(1, \dots 1)$). The leading eigenstate (the one with the largest eigenvalue, which dominates the final state of the scattering process), denoted with the blue line, consists mainly of short partitions for $p = 8.1, 12.1$, becomes approximately equipartitioned for momenta $p = 14.1, 15.1$, which we identify with the crossover scale p_c, and consists mainly of long partitions for $p = 16.1, 20.1$. The eigenstates with $n = 10, 30$ behave in a more or less complementary way, although for them the trends are less clear.

contribute to the dynamics can also be seen from the plot of absolute values of the S-matrix elements (Fig. 4.2).

Now that we have the eigenvalues, we can explore whether the S-matrix follows the RMT prediction for quantum chaotic scattering, which implies that the eigenphases behave essentially like eigenenergies of a bound system and thus should be described by Gaussian random ensembles. We fit the distribution of normalized spacings to (1.7) with β being the fitting parameter, and compare the outcome to the curve with $\beta = 1$ which one could expect from the time-reversal-symmetric nature of our scattering problem (Fig. 4.3). There is a significant population of eigenphase spacings far from zero (which is what we expect from Wigner-Dyson distributions), but also a non-vanishing set of spacings close to zero (which happens with the Poisson distribution but not with Wigner-Dyson curves which always vanish at zero spacing, due to level repulsion). We can thus tentatively conclude that the HES scattering exhibits a mixed state space, with both regular (Poisson) and chaotic (Wigner-Dyson) channels. There is however the caveat that for $N \approx 10$ the set of spacings available for the accessible levels is rather small, so it is hard to make robust statements about the distribution.

4.2 Phenomenology of closed string scattering

As we have mentioned, closed HES amplitudes are obtained from the st and tu contributions to the open HES amplitudes by the use of KLT relations. Diagonalization of the resulting S-matrices is greatly simplified by the direct product structure of the KLT

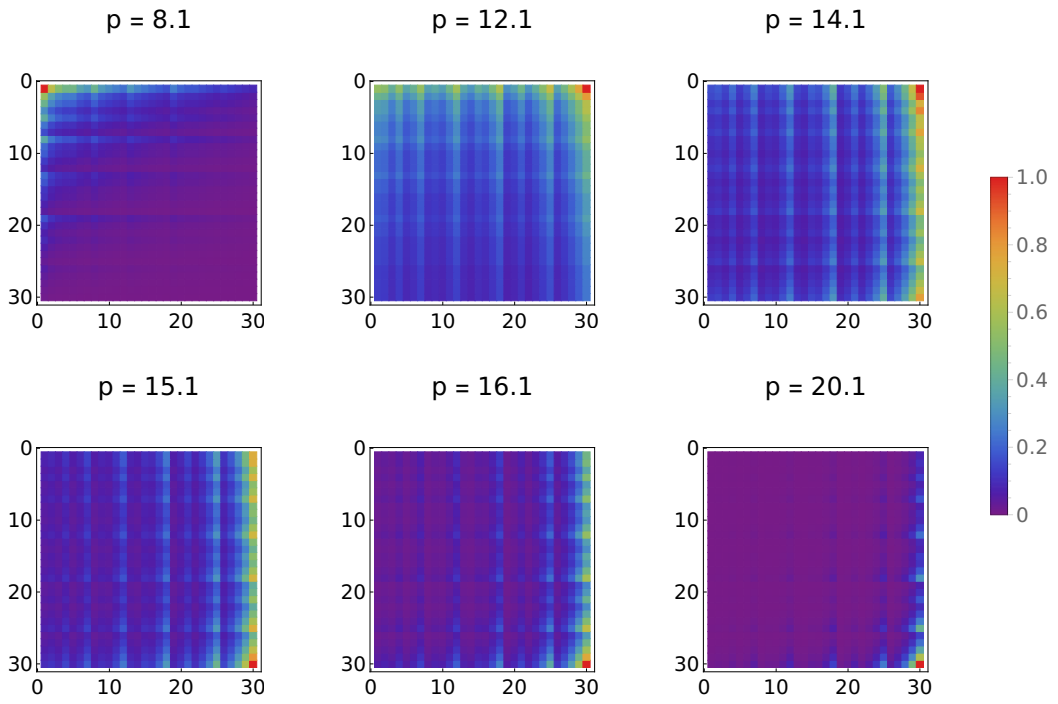

Figure 4.2: The S-matrix in the partition basis for the same kinematics as in Fig. 4.1, the color code showing the module of the (generically complex) matrix elements, from smallest (purple) to largest (red) (normalized by the matrix element with the highest magnitude). In accordance with the previous figure, the dominant processes for $p < p_c \approx 15$ involve short partitions with few occupied levels but with large occupation numbers (upper left corner), whereas for $p < p_c$ the opposite is true and the lower left corner of the S-matrix is dominant.

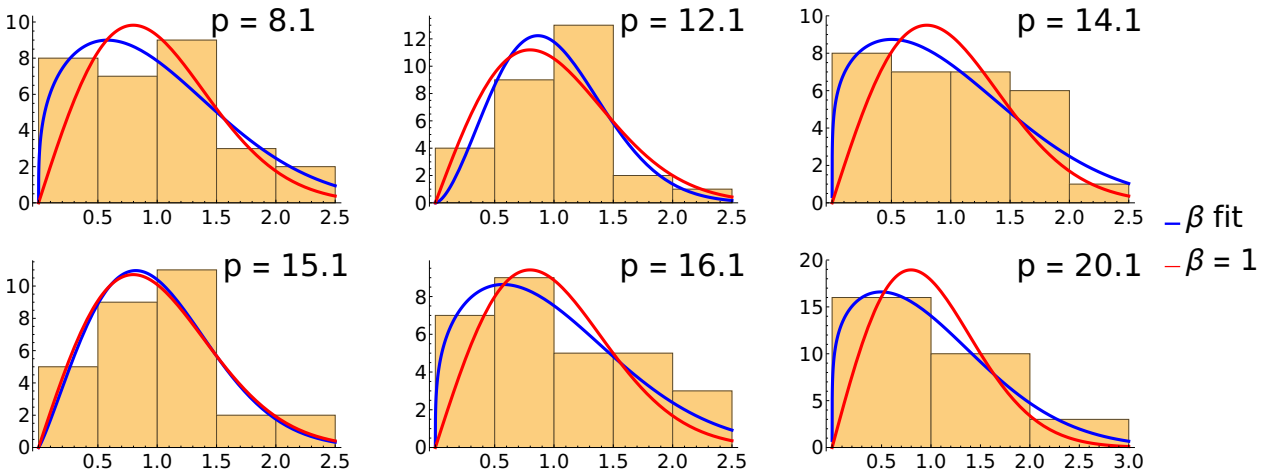

Figure 4.3: Normalized eigenphase spacing distribution for the same kinematics as in Fig. 4.1. The blue line represents the best fit to the Wigner-Dyson distribution (1.7) while the red line corresponds to the GOE ($\beta = 1$) prediction expected from the time-reversal symmetry. There is a significant portion of non-zero spacings as predicted by the RMT, but also a non-vanishing set of spacings close to zero. This suggests that dynamics is mixed, consisting of contributions from both Poisson and Wigner-Dyson distribution.

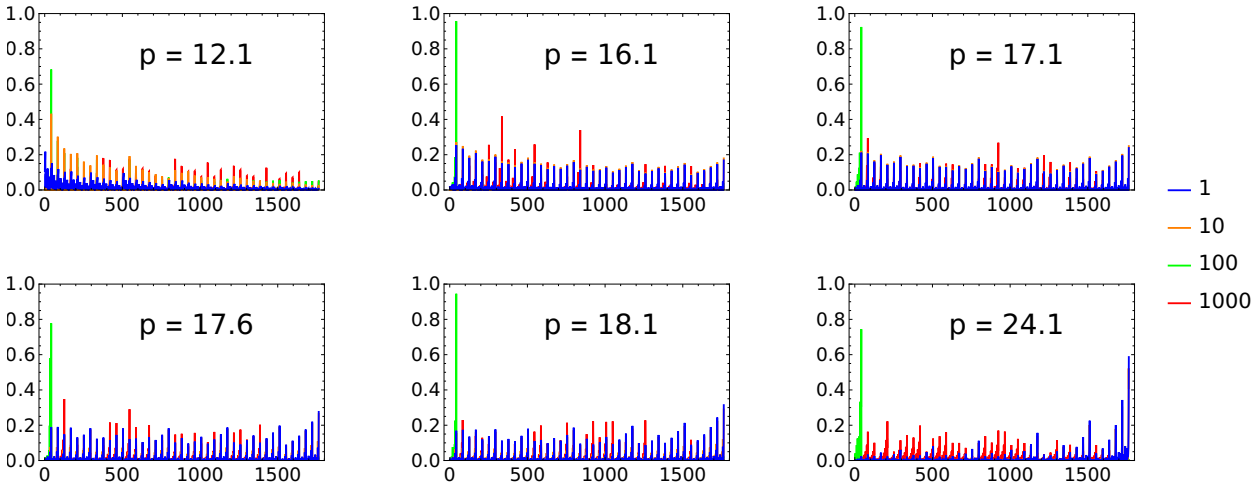

Figure 4.4: Coefficients of the closed string S-matrix eigenvector no. n in the partition basis, for $n = 1, 10, 100, 1000$ (blue, orange, green, red) and six momentum values $p = 12.1, 16.1, 17.1, 17.6, 18.1, 24.1$ assuming $N = 10$, $\theta = 0.2$, $\theta' = 0.3$ and $\phi' = 0.2$. Overall behavior is similar as for the open string (compare to Fig. 4.1) although the much larger state space makes visual inspection somewhat harder. Nevertheless, the crossover from mainly short to mainly long partitions is again clear, with $p_c \approx 17.5$.

relations for four-leg amplitudes [43].

Just as in the case of open strings, we observe the crossover from predominantly small to predominantly large partitions and the similar dependence of p_c on the angles as for open strings (Fig. 4.4).

The big difference from the open string case is the size of the S-matrices for given setup (e.g. for $N = 10$, for the open string we obtain a square matrix with $p(N) = 42$ rows and columns, while for the closed string this number is $p(N)^2 = 1724$). Due to larger size of the matrix we are now in better position to test the eigenphase spacing statistics and we find (Fig. 4.6) that the RMT predictions are in decent agreement with the observed spacing distribution (i.e., we clearly identify level repulsion).

The RMT description seems to work best for $p \sim p_c$ while for both lower and higher energies sharp peaks and holes in the distribution spoil the agreement with the Wigner-Dyson distribution. This can be understood as the competition of two opposite effects. First, as we increase the energy more and more modes are activated providing more channels for the interaction, forming a complex structure through which chaotic behavior may develop. On the other hand, at high energies there is "less time" for the interaction to occur, the strings just "fly away from each other", which results in the suppression of the chaotic behavior. Hence it is indeed expected that chaos will be most evident in some range of energies close to the p_c. This situation is analogous to classical scattering, where likewise at low energies the skeleton of periodic orbits (which defines the symbolic dynamics) is quite simple as most orbits see just a near-harmonic potential well, at high energies most orbits barely feel the scattering potential and continue to infinity almost undisturbed, and at intermediate energies the competition between the bounded and unbounded dynamics generates sensitivity to initial conditions and chaos.

We further support the above reasoning by calculating the information entropy associated with the S-matrix using 3.38. As seen from Fig. 4.7, the entropy admits a maximum at the crossover, indicating increase in the dynamics complexity.

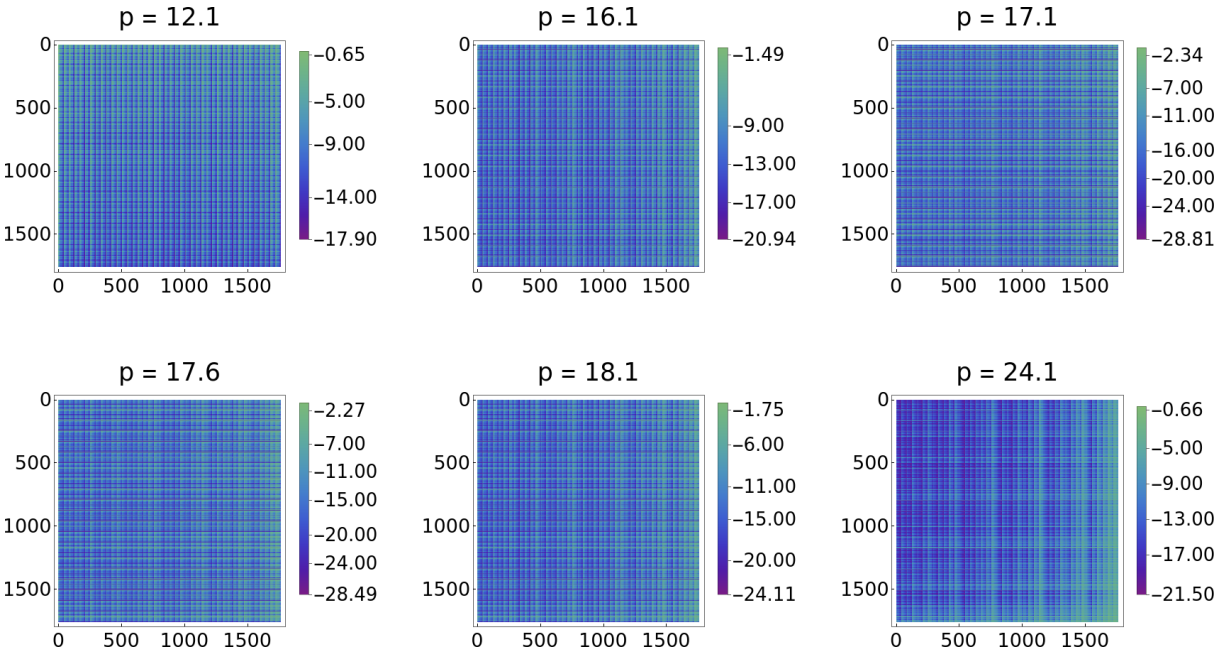

Figure 4.5: The logarithm of the S-matrix for the closed string in the partition basis for the same kinematics as in Fig. 4.4, the color code showing the module of the (generically complex) matrix elements, from smallest (dark blue) to largest (green) (normalized by the matrix element with the highest magnitude). In accordance with the previous figure, we observe the crossover from short to long partitions dominating the dynamics (similar to Fig. 4.2).

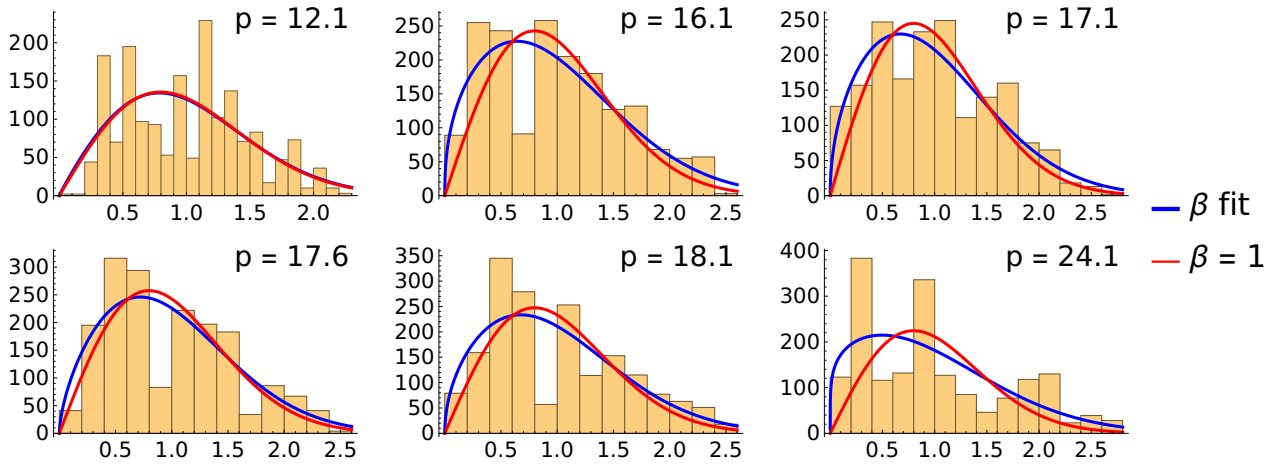

Figure 4.6: The normalized eigenphase spacing distribution for the same kinematics as in Fig. 4.4. The blue line represents the best fit to 1.7 while the red line corresponds to the GOE ($\beta = 1$) predictions expected from the time-reversal symmetry. The distributions seem to be in better agreement with the RMT predictions near the crossover (e.g. $p \in \{17.1, 17.6, 18.1\}$) but in general there are some deviations in terms of peaks and holes. Distributions clearly favor non-zero spacings.

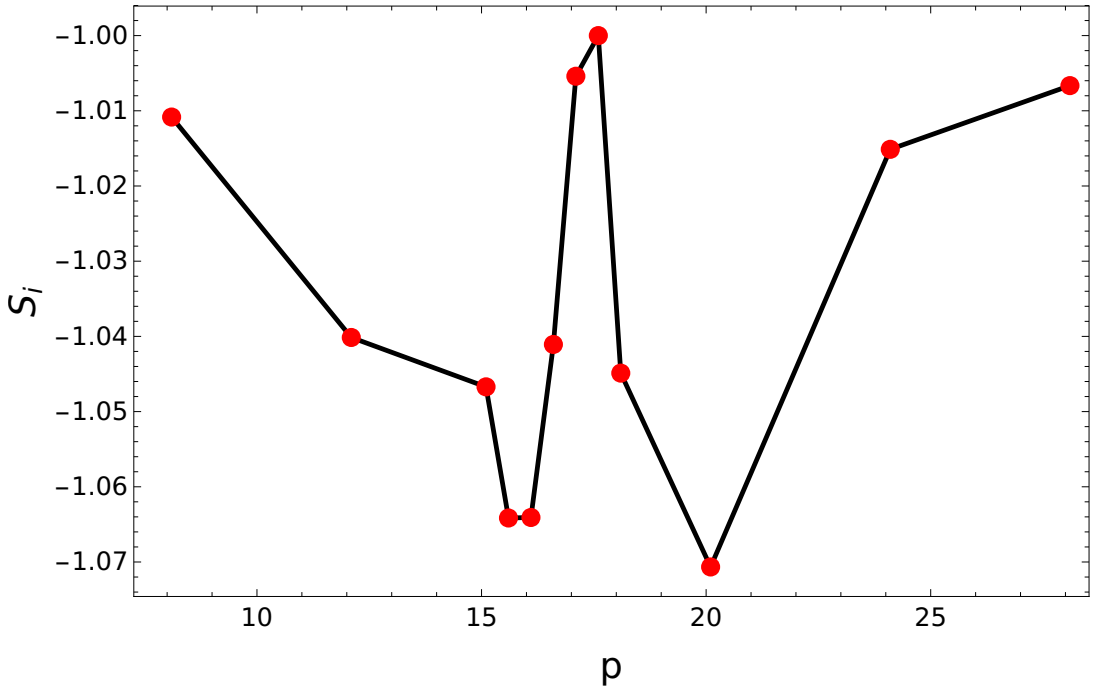

Figure 4.7: Shannon information entropy normalized by the absolute value of the maximum entropy for the same kinematics as in Fig. 4.4. We observe a sharp peak in the entropy at the crossover momentum $p_c \approx 17.5$. The line is just to guide the eye.

We note that st and tu parts of the open string amplitude in this case behave quite differently, as demonstrated in Fig. 4.8. In the tu matrix structure we find stripes which became denser after the crossover, while in the st part we do not see any obvious signs of the crossover. The fact that these two contributions to the amplitude have very different structures implies that one should be cautious in making conclusions about the whole amplitude by studying one of the channels [24, 47].

The behavior of phases of the $\mathcal{A}_{tu}$ matrices induces similar structure in the complete S-matrix. As seen from Fig. 4.9, stripes in the phases of the S- matrix became denser at the crossover.

Finally, we see no sign of the string/BH transition in our calculations, most likely because the levels we can consider are not high enough.

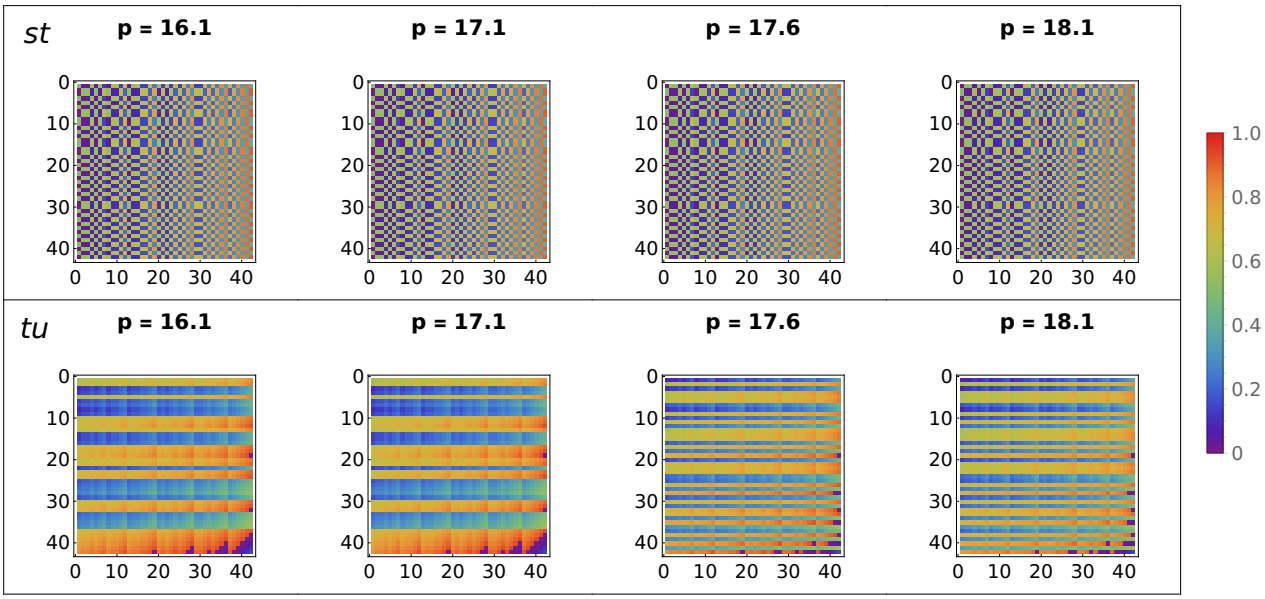

Figure 4.8: Channels $\mathcal{A}_{st}$ and $\mathcal{A}_{tu}$ of the open string amplitude in the partition basis for the same kinematics as in Fig. 4.4, the color code showing the phases of the elements, normalized to the $[-1, 1]$ interval. The tu part shows stripes (i.e., sets of partitions with lengths confined to some fixed interval) of real elements whose number increases at the crossover. The phase structure of the st part is on the other hand more or less featureless, and exhibits no clearly visible changes at the crossover.

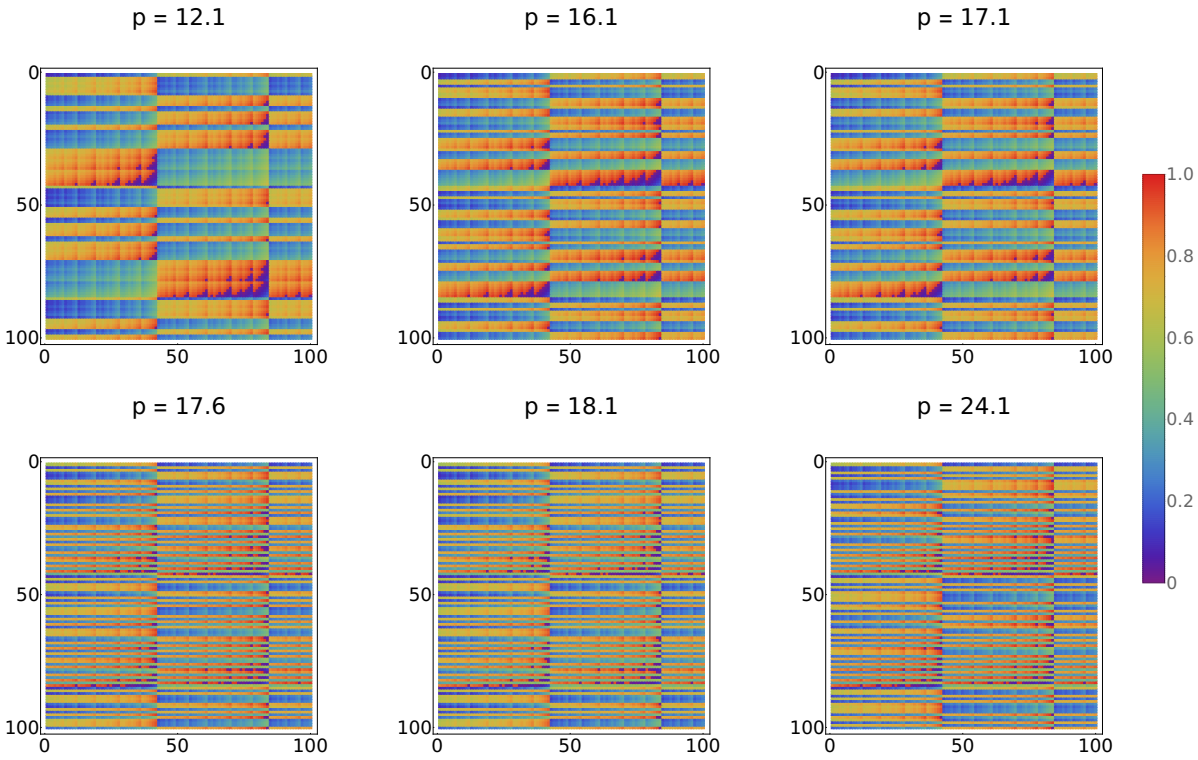

Figure 4.9: S-matrices for closed strings in the partition basis for the same kinematics as in Fig. 4.4, the color code showing the phases of the elements, normalized to the interval [-1,1]. We identify the same striped structure as in Fig. 4.8. The number of stripes increases at the crossover. Only a part of the S-matrix is shown in order to zoom-in into the stripe structure; the rest of the S-matrix behaves in a similar manner.

Chapter 5

Conclusions

In this thesis we have studied the scattering of highly excited strings both in the classical and in the quantum regime. The chaotic nature of BHs and the BH/string correspondence have motivated us to first investigate the signs of chaos in the classical string scattering off the BH, and then also to look in detail at the quantum S-matrix elements for the processes including HES. The quantum case provides a way to study the chaotic behavior of BHs in the perturbative string theory framework and importantly provides an example of a quantum field theory in which the signs of chaos can be probed analytically. Therefore, even independently of the string/BH complementarity, it is instructive to look at the sings of chaos in string scattering: (1) it is a little-studied but important aspect of string theory (2) it is a rare example of tractable dynamics (in the regime of small string coupling g) in a strongly nonlinear field theory (3) it provides insight into the mechanisms of chaos in conformal field theories (CFT), as string theory is really a CFT on the worldsheet.[1]

Our calculations of open and closed string scattering amplitudes involving two HES and two tachyon states enable us to draw the following conclusions regarding the phenomenology of the HES scattering:

1. In both open and closed case we observe the transition from short to long partitions dominating the dynamics. We identify this smooth transition at energies corresponding to the momentum p_c when short and long partitions are equally contributing to the dynamics.

2. For the open string we find the comparison of the S-matrix eigenphases with the RMT predictions inconclusive because of the small dimensions of matrices we can numerically achieve.

3. For the closed string we find clear evidence of level repulsion, the robust prediction of the RMT. Because here the dimensions of the S-matrices we can achieve are significantly larger, we are able to find a decent agreement of the spacing distribution with the RMT predictions, although there are still some deviations. The deviations may be a consequence of the mixed state space, containing both the regions with regular and chaotic dynamics and/or due to the presence of additional symmetry.

[1] While recent studies of chaos and time-disordered correlators in AdS/CFT [2, 3, 48, 49] have brought much information on chaos in holographic "CFTs", they typically consider the situation when either a finite temperature T or some other operator (usually chemical potential μ) breaks conformal invariance. In such CFTs, there is typically no chaos at all when $T = \mu = 0$, which is very different from string theory, i.e. the worldsheet CFT defined by the Polyakov action that we study.

4. We see no signs of the transition to the effective BH description in our analysis. It may well be that the levels we were able to analyse here are simply not high enough.

5. In the classical setting we consider for comparison (the closed string scattering off the BH in the Minkowski background) we find the extreme sensitivity of the final state to the initial conditions, in agreement with the chaotic behavior of this system established in the literature.

We observe that the scattering of closed strings shows systematic deviations from the GOE distribution which one would expect from the TRS of this integer-spin system. This could be explained by the symmetry between the left- and right-moving modes of the closed string (which has no analogy for the open string). That is, after switching partitions corresponding to the left- and right-moving modes, we should obtain the same amplitude. This symmetry induces additional correlation between the eigenphases and could explain the deviation from the GOE ensemble. Being realized as a unitary operator, and because it is an involution, this symmetry classifies eigenstates as being even or odd under the exchange of left- and right-moving modes. Hence, in order to remove correlations due to this symmetry, one should perform the comparison to the GOE predictions for two sets of eigenphases *separately*, one for odd and other for even eigenstates. This procedure is commonly refered to as 'unfolding' of the spectrum in the context of the RMT. Although performing this is simple in the basis of partitions, the KLT relations which we utilize provides us with the closed strings S-matrix in a different basis. This can be easily seen from Eq. (3.29): the exchange of partitions in the two open string factors does not give the same closed amplitude as one factor is the st and other is the tu part of the open string amplitude. This is also evident from the substitution used to factorize the integration from the closed string worldsheet to the product of integrations forming the open string amplitudes in the original derivation of the KLT relations [41]. Nevertheless, this substitution only shuffles the states belonging to the subset of the states with fixed partition length, as the partition length is counted by the polarization factors, which are intact under the substitution. Hence, the lengths of the partitions are the same both in the original partition basis, and in the basis obtained from the KLT direct product structure (at least in the four-leg process).

In order to separate the states into even and odd, one should find the S-matrix in the basis of partitions (e.g. through the use of the DDF formalism [29]). We expect improved agreement with the GOE predictions after this separation is performed, enabling a robust testing of the chaoticity of this process (e.g. probing the portion of the state space admitting regular dynamics). We leave the improvements of the RMT analysis along these lines for future work.

Furthermore, it would be of great interest to compare the classical setting from chapter 2 to the analysis of the S-matrix in chapter 4. This is a nontrivial task because the classical setup is described by canonical variables (e.g. $r(\tau), p_r(\tau)$) in a special axial-symmetric configuration, while in the quantum case, besides the momenta and angles, we need also the partitions to specify the process; in other words, the quantum case corresponds to arbitrary and time-dependent shapes of the closed string (determined by the mode expansion), unlike the classical configuration which is chosen is such a way to give a circular string in axial-symmetric configuration.

The comparison at the level of partitions can be accomplished by exciting particular modes in the classical string, but this would demand giving up the axial symmetry, making

the integration of the equations of motion much more complicated. In order to mimic the classical states, one should in principle consider the scattering of the *coherent* states (in addition to taking the large N limit). One could try to find the coherent state vertex for a single mode or for several modes (as performed in [50] through the DDF formalism [29]), calculate the scattering amplitude and try to compare the final state of classical and quantum setup in the collinear limit ($\theta = 0, \theta' \in \{0, \pi\}$). This comparison may be performed by calculating the amplitude for the forward scattering ($\theta' = \pi$) and for backscattering ($\theta' = \pi$) and taking the larger amplitude to determine the final state. One may hope that even the states which are not coherent allow for such comparison in the setting described here (and, again, for sufficietly large N), but as we explained at the end of subsection 3.1.1, the amplitude is exactly zero for both collinear configurations. A less direct comparison could be performed by considering the topological entropy both for quantum and classical scattering. For the latter, one needs to find the appropriate symbolic dynamics for the classical case. In addition, one could search for the equivalent of p_c in the classical scattering. We hope to report on the relation of quantum and classical cases in our future work.

.

Bibliography

[1] Yasuhiro Sekino and Leonard Susskind. Fast Scramblers. *JHEP*, 10:065, 2008.

[2] Daniel A. Roberts, Douglas Stanford, and Leonard Susskind. Localized shocks. *JHEP*, 03:051, 2015.

[3] Stephen H. Shenker and Douglas Stanford. Stringy effects in scrambling. *JHEP*, 05:132, 2015.

[4] Juan Maldacena, Stephen H. Shenker, and Douglas Stanford. A bound on chaos. *JHEP*, 08:106, 2016.

[5] Juan Maldacena and Douglas Stanford. Remarks on the Sachdev-Ye-Kitaev model. *Phys. Rev. D*, 94(10):106002, 2016.

[6] Nima Lashkari, Douglas Stanford, Matthew Hastings, Tobias Osborne, and Patrick Hayden. Towards the Fast Scrambling Conjecture. *JHEP*, 04:022, 2013.

[7] Pierre Gaspard. Chaos, scattering, and statistical mechanics. Cambridge nonlinear science series ; 9, Cambridge, U.K. ;, 1998. Cambridge University Press.

[8] Jürgen Vollmer, László Mátyás, and Tamás Tél. *Journal of Statistical Physics*, 109(3/4):875–893, 2002.

[9] Vito Latora and Michel Baranger. Kolmogorov-sinai entropy rate versus physical entropy. *Phys. Rev. Lett.*, 82:520–523, Jan 1999.

[10] E Doron and U Smilansky. Semiclassical quantization of chaotic billiards: a scattering theory approach. *Nonlinearity*, 5(5):1055, sep 1992.

[11] Reinhold Blümel, Barbara Dietz, Christof Jung, and Uzy Smilansky. On the transition to chaotic scattering. *Journal of Physics A*, 25:1483–1502, 1992.

[12] Leonard Susskind. Some speculations about black hole entropy in string theory. pages 118–131, 10 1993.

[13] Gary T. Horowitz and Joseph Polchinski. A Correspondence principle for black holes and strings. *Phys. Rev. D*, 55:6189–6197, 1997.

[14] Gary T. Horowitz and Joseph Polchinski. Selfgravitating fundamental strings. *Phys. Rev. D*, 57:2557–2563, 1998.

[15] George E. Andrews. *The theory of partitions / George E. Andrews.* Addison-Wesley Pub. Co., Advanced Book Program Reading, Mass, 1976.

[16] Albert Einstein. Zum Quantensatz von Sommerfeld und Epstein. *Deutsche Physikalische Gesellschaft, Verhandlungen*, 19:82, 1917.

[17] Fritz Haake. *Quantum Signatures of Chaos*, pages 583–595. Springer US, Boston, MA, 1991.

[18] Madan Lal Mehta. *Random Matrices*. 3rd edition, 2004.

[19] Alexander Altland and Martin R. Zirnbauer. Nonstandard symmetry classes in mesoscopic normal-superconducting hybrid structures. *Physical Review B*, 55:1142–1161, 1996.

[20] C. W. J. Beenakker. Random-matrix theory of Majorana fermions and topological superconductors. *Rev. Mod. Phys.*, 87:1037, 2015.

[21] David J. Gross and Vladimir Rosenhaus. Chaotic scattering of highly excited strings. *JHEP*, 05:048, 2021.

[22] Vladimir Rosenhaus. Chaos in the Quantum Field Theory S-Matrix. *Phys. Rev. Lett.*, 127(2):021601, 2021.

[23] Maurizio Firrotta and Vladimir Rosenhaus. Photon emission from an excited string. *JHEP*, 09:211, 2022.

[24] Vladimir Rosenhaus. Chaos in a Many-String Scattering Amplitude. *Phys. Rev. Lett.*, 129(3):031601, 2022.

[25] Massimo Bianchi, Maurizio Firrotta, Jacob Sonnenschein, and Dorin Weissman. Measure for Chaotic Scattering Amplitudes. *Phys. Rev. Lett.*, 129(26):261601, 2022.

[26] Massimo Bianchi, Maurizio Firrotta, Jacob Sonnenschein, and Dorin Weissman. Measuring chaos in string scattering processes. 3 2023.

[27] Maurizio Firrotta. The chaotic emergence of thermalization in highly excited string decays. 1 2023.

[28] Koji Hashimoto, Yoshinori Matsuo, and Takuya Yoda. Transient chaos analysis of string scattering. *JHEP*, 11:147, 2022.

[29] Dimitri Skliros and Mark Hindmarsh. String Vertex Operators and Cosmic Strings. *Phys. Rev. D*, 84:126001, 2011.

[30] Andrei V. Frolov and Arne L. Larsen. Chaotic scattering and capture of strings by black hole. *Class. Quant. Grav.*, 16:3717–3724, 1999.

[31] S. S. Gubser, I. R. Klebanov, and Alexander M. Polyakov. A Semiclassical limit of the gauge / string correspondence. *Nucl. Phys. B*, 636:99–114, 2002.

[32] Yuhma Asano, Daisuke Kawai, Hideki Kyono, and Kentaroh Yoshida. Chaotic strings in a near Penrose limit of $AdS_5 \times T^{1,1}$. *JHEP*, 08:060, 2015.

[33] Leopoldo A. Pando Zayas and Cesar A. Terrero-Escalante. Chaos in the Gauge / Gravity Correspondence. *JHEP*, 09:094, 2010.

[34] Pallab Basu and Leopoldo A. Pando Zayas. Analytic Non-integrability in String Theory. *Phys. Rev. D*, 84:046006, 2011.

[35] Pallab Basu, Pankaj Chaturvedi, and Prasant Samantray. Chaotic dynamics of strings in charged black hole backgrounds. *Phys. Rev. D*, 95(6):066014, 2017.

[36] Pallab Basu and Leopoldo A. Pando Zayas. Chaos rules out integrability of strings on $AdS_5 \times T^{1,1}$. *Phys. Lett. B*, 700:243–248, 2011.

[37] Leopoldo A. Pando Zayas and Cesar A. Terrero-Escalante. Chaos in the Gauge / Gravity Correspondence. *JHEP*, 09:094, 2010.

[38] Takaaki Ishii, Keiju Murata, and Kentaroh Yoshida. Fate of chaotic strings in a confining geometry. *Phys. Rev. D*, 95(6):066019, 2017.

[39] Tristan McLoughlin and Anne Spiering. Chaotic spin chains in AdS/CFT. *JHEP*, 09:240, 2022.

[40] Mihailo Čubrović. The bound on chaos for closed strings in Anti-de Sitter black hole backgrounds. *JHEP*, 12:150, 2019.

[41] H. Kawai, D.C. Lewellen, and S.-H.H. Tye. A relation between tree amplitudes of closed and open strings. *Nuclear Physics B*, 269(1):1–23, 1986.

[42] Thomas Sondergaard. Perturbative Gravity and Gauge Theory Relations: A Review. *Adv. High Energy Phys.*, 2012:726030, 2012.

[43] Stephan Stieberger and Tomasz R. Taylor. Closed String Amplitudes as Single-Valued Open String Amplitudes. *Nucl. Phys. B*, 881:269–287, 2014.

[44] E Del Giudice, P Di Vecchia, and S Fubini. General properties of the dual resonance model. *Annals of Physics*, 70(2):378–398, 1972.

[45] Massimo Bianchi and Maurizio Firrotta. DDF operators, open string coherent states and their scattering amplitudes. *Nucl. Phys. B*, 952:114943, 2020.

[46] Zvi Bern, John Joseph M. Carrasco, and Henrik Johansson. Perturbative quantum gravity as a double copy of gauge theory. *Phys. Rev. Lett.*, 105:061602, Aug 2010.

[47] Koji Hashimoto and Norihiro Tanahashi. Universality in Chaos of Particle Motion near Black Hole Horizon. *Phys. Rev. D*, 95(2):024007, 2017.

[48] Sašo Grozdanov, Koenraad Schalm, and Vincenzo Scopelliti. Black hole scrambling from hydrodynamics. *Phys. Rev. Lett.*, 120(23):231601, 2018.

[49] Ben Craps, Marine De Clerck, Philip Hacker, Kévin Nguyen, and Charles Rabideau. Slow scrambling in extremal BTZ and microstate geometries. *JHEP*, 03:020, 2021.

[50] Mark Hindmarsh and Dimitri Skliros. Covariant Closed String Coherent States. *Phys. Rev. Lett.*, 106:081602, 2011.